Supporting Information for

Planar lithium deposition/dissolution enabling practical 500 Wh kg^{-1} anode-free pouch cells

Lei Liu[1,2,3], Yuxuan Xiang[1,2,3], Xingyu Lu[1,5], Jianhui Wang[1,2,3,4]*

[1]Research Center for Industries of the Future (RCIF), Westlake University, Hangzhou 310030, China.

[2]Zhejiang Key Laboratory of 3D Micro/Nano Fabrication and Characterization, School of Engineering, Westlake University, Hangzhou 310030, China.

[3]Institute of Advanced Technology, Westlake Institute for Advanced Study, Hangzhou 310024, China.

[4]Division of Solar Energy Conversion and Catalysis at Westlake University, Zhejiang Baima Lake Laboratory Co. Ltd., Hangzhou 310000, China

[5]Instrumentation and Service Center for Molecular Sciences, Westlake University, Hangzhou 310030, China.

*Corresponding Author: Jianhui Wang

wangjianhui@westlake.edu.cn

Contents

1. Supplementary figures 4

Supplementary Figure 1. Physicochemical properties of the LiDFOB/NDFA electrolytes dependent of salt concentrations. 4

Supplementary Figure 2. Electrochemical stability of the LiDFOB/NDFA electrolytes dependent of salt concentrations. 5

Supplementary Figure 3. Battery performances using the LiDFOB/NDFA electrolytes dependent of salt concentrations. 6

Supplementary Figure 4. Initial charge-discharge profiles of Cu||NCM811 pouch cells using different electrolytes and areal capacities. 7

Supplementary Figure 5. Cross-section and 3D-reconstruction views of 5th deposited Li collected at 4.4 V from Cu||NCM811 pouch cells (5.6 mAh cm^{-2}) using different electrolytes. 8

Supplementary Figure 6. 2D GIXD analysis of 5th deposited Li collected at 4.4 V from Cu||NCM811 pouch cells (5.6 mAh cm^{-2}) using different electrolytes. 9

Supplementary Figure 7. Morphology evolution of 1st deposited/dissolved Li in Cu||NCM811 pouch cells (5.6 mAh cm^{-2}) using different electrolytes. 10

Supplementary Figure 8. Oblique angle large-view SEM images of 1st dissolved Li in BAFF. 11

Supplementary Figure 9. Morphology evolution of 5th deposited/dissolved Li in Cu||NCM811 pouch cells (5.6 mAh cm^{-2}) using different electrolytes. 12

Supplementary Figure 10. Oblique angle large-view SEM images of 5th dissolved Li in BAFF. 13

Supplementary Figure 11. AFM results of 5th deposited Li in AFE and HCDE. 14

Supplementary Figure 12. XPS spectra of BAFF-derived SEI. 15

Supplementary Figure 13. MALDI-TOF spectrum of BAFF-derived SEI. 16

Supplementary Figure 14. ss-NMR analysis for BAFF-derived SEI. 17

Supplementary Figure 15. Cycling performances of 2.7Ah Cu||NCM811 pouch cells using BAFF at different DoD. 18

Supplementary Figure 16. Cycling performances of 6.4Ah Cu||NCM811 pouch cells using BAFF. 19

Supplementary Figure 17. Cycling performances of 2.7Ah Cu||NCM811 pouch cells using different electrolytes. 20

Supplementary Figure 18. Comparison of state-of-the-art Ah-level high-energy-density anode-free Li pouch cells in literature and this work. 21

Supplementary Figure 19. Comparison in morphology and reversible capacity of NCM811 cathode (5.6 mAh cm^{-2}) before and after cycling. 22

Supplementary Figure 20. MST quantitative analysis of inactive Li metal and LiH in 2.7 Ah Cu||NCM811 pouch cells with 80% capacity retention. 23

2. Supplementary tables 24

Supplementary Table 1 Battery price per kWh of LIBs, LMBs and AFLMBs. 24

Supplementary Table 2 Commercially available components for Li-ion batteries. 25

Supplementary Table 3 Correlation of cell parameters and energy density for Graphite||NCM Li-ion pouch cell. 30
Supplementary Table 4 Correlation of cell parameters and energy density for Cu||NCM anode-free lithium pouch cell..... 26
Supplementary Table 5 Physicochemical properties of LiDFOB/NDFA electrolytes at 25℃..... 32
Supplementary Table 6 Cell parameters of home-made 2.7 Ah anode-free lithium pouch cell. 33
Supplementary Table 7 Comparison of Ah-level high-energy-density anode-free Li pouch cells in literature and this work. 34
Supplementary Table 8 Energy density and power density of home-made anode-free Li pouch cells and representative commercial energy storage devices. 35
3. Supplementary references..... 37

Supplementary figures

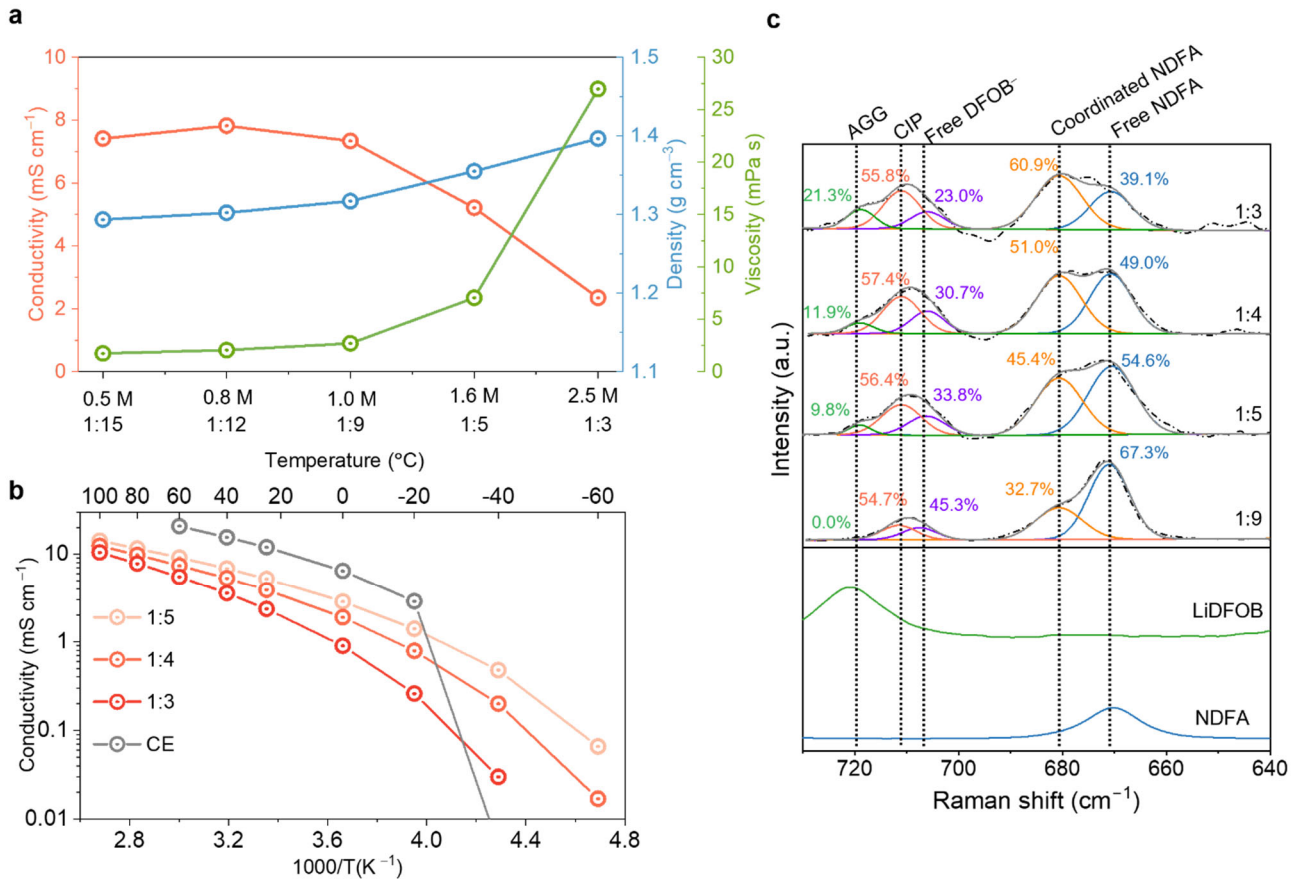

Supplementary Figure 1. Physicochemical properties of the LiDFOB/NDFA electrolytes dependent of salt concentrations. (a) Viscosity, density and ionic conductivity of various concentration electrolytes at 25 ℃. (b) Ionic conductivity for 1.6 M LiDFOB/NDFA (BAFF) at different temperatures. (c) Raman spectra of various concentrations of LiDFOB/NDFA electrolytes. Pure LiDFOB salt and NDFA solvent were used as references.

With a moderate salt concentration of 1.6 M, the BAFF electrolyte demonstrates good ionic conductivities (0.5 ~ 14.2 mS cm^{-1}) in the wide temperature ranges from -40 to 100 ℃. From the Raman results, the major species in BAFF are coordinated $DFOB^-$ anions (66.2%) and free-state NDFA solvents (54.6%).

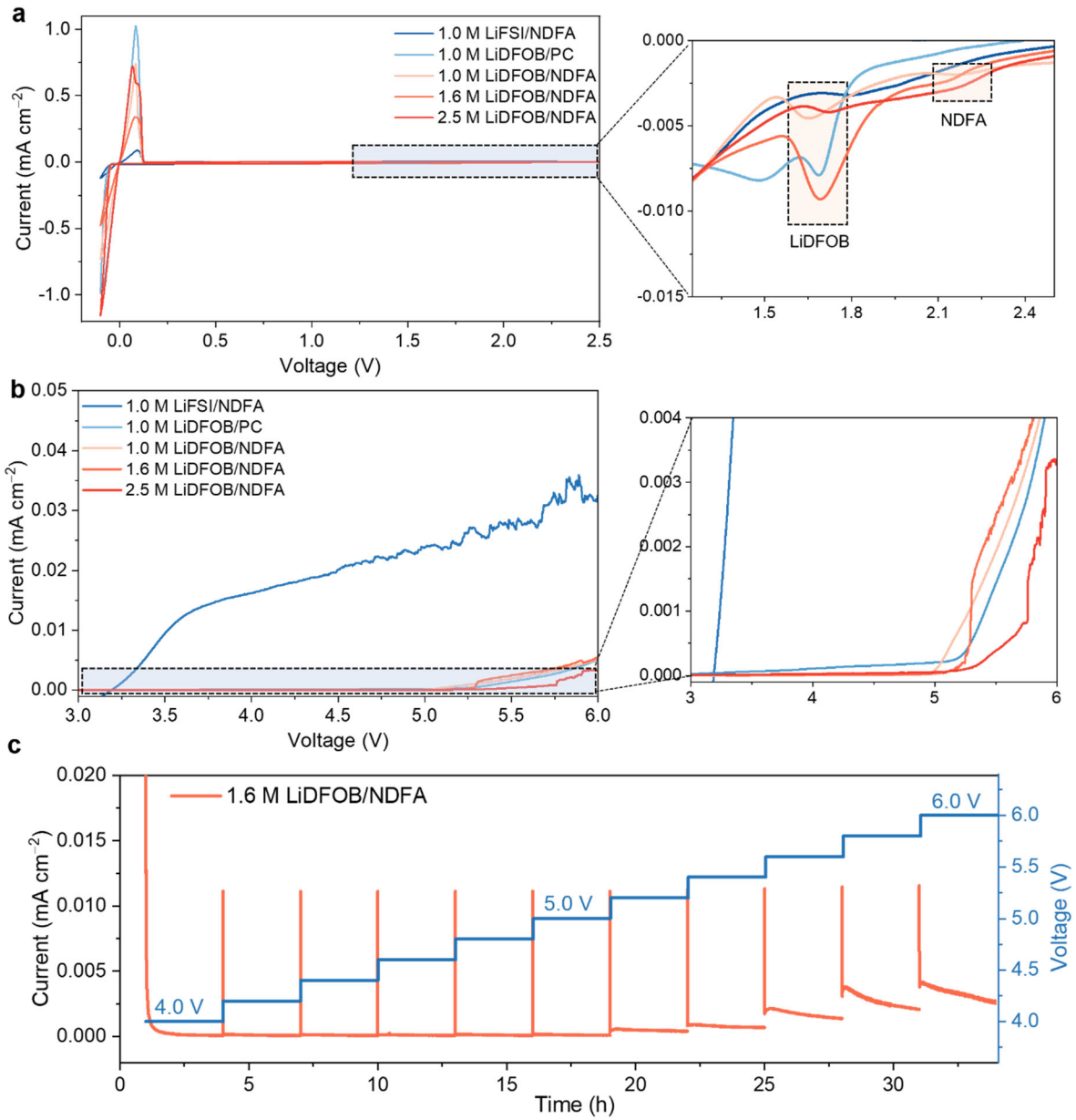

Supplementary Figure 2. Electrochemical stability of the LiDFOB/NDFA electrolytes dependent of salt concentrations. (a) Cyclic voltammetry (CV) in Li||Cu coin cells. (b) Linear sweep voltammetry (LSV) in Li||Al coin cells. (c) Potentiostatic polarization in Li||Al coin cell using BAFF. The electrolytes of 1.0M LiFSI/NDFA and 1.0M LiDFOB/PC were used as references.

The BAFF electrolyte shows a wide electrochemical stability window of ~5 V. During the cathodic scan, BAFF successively undergoes reductive decompositions of NDFA at ~2.2 V vs Li^+/Li and $DFOB^-$ at 1.7 V vs Li^+/Li, evidencing that both NDFA solvent and LiDFOB salt contribute to SEI formation. This mechanism could be associated with the electrolyte solution structure, wherein the contents of coordinated $DFOB^-$ anions and free-state NDFA solvents take the major part. For the anodic polarization, the presence of LiDFOB in the electrolyte efficiently passivates the Al electrode and suppresses Al dissolution at high voltages. Almost no leakage current density can be detected up to 5 V even under a harsh potentiostatic polarization, suggesting a high stability of BAFF at high voltages.

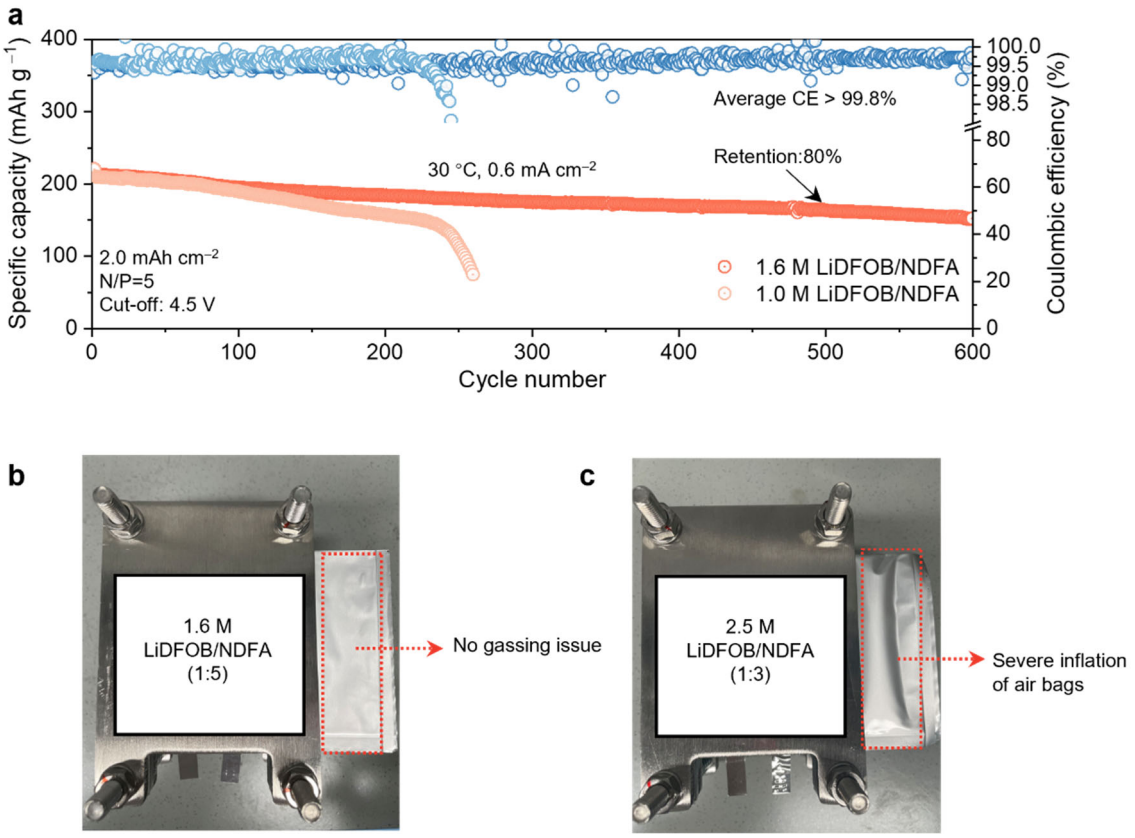

Supplementary Figure 3. Battery performances using the LiDFOB/NDFA electrolytes dependent of salt concentrations (a) Long-term cycling performances of 50 μm-Li||NCM811 coin cells. N/P ratio is 5. The amount of electrolyte was 60 μL per cell. (b,c) Photographs of anode-free Li pouch cells using (c) 1.6 M and (d) 2.5 M LiDFOB/NDFA electrolytes after 30 cycles.

For the LiDFOB/NDFA electrolytes, the higher concentration electrolyte (1.6 M) shows a better cycling stability of 50 μm-Li||NCM811 coin cells as compared to the lower one (1.0 M). However, the usage of an even higher salt concentration (2.5 M) brings a severe gassing issue, which is not favorable for the battery safety and long-term stability in the practical applications. The moderate concentration of 1.6 M LiDFOB/NDFA (BAFF) shows both high stability and no gassing during cycling, and thus, is selected for detail investigation in this work.

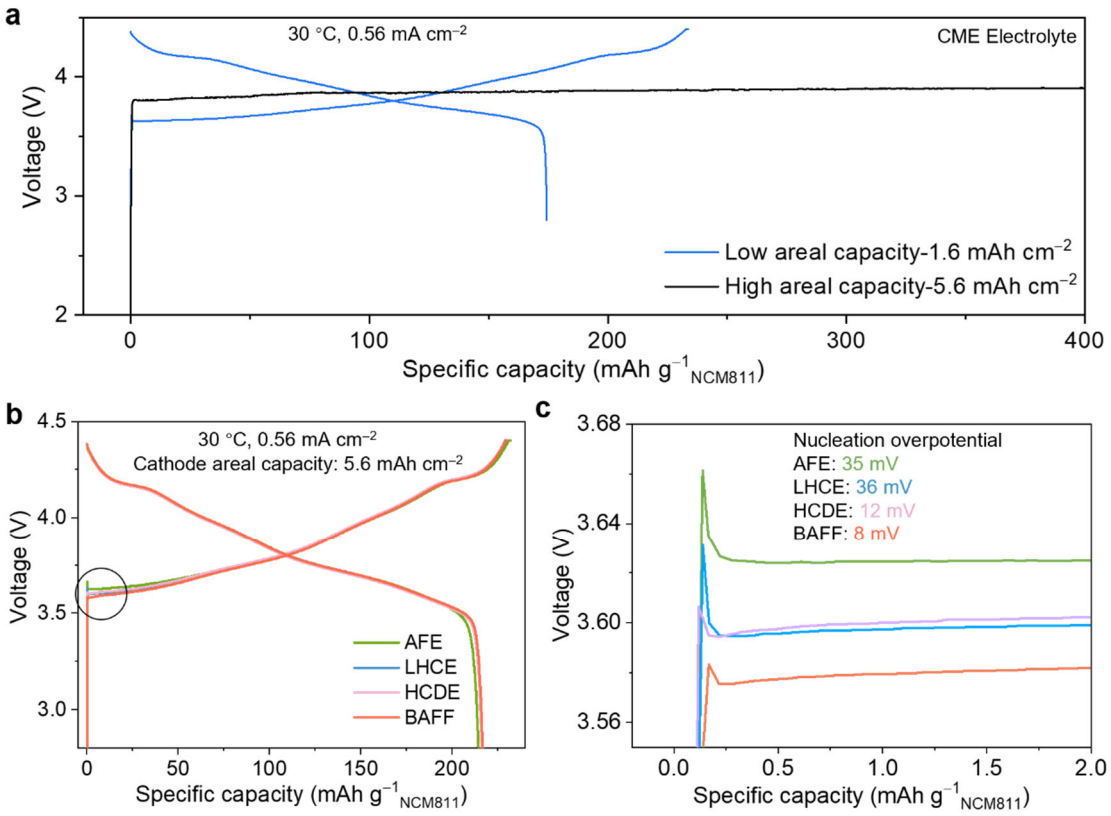

Supplementary Figure 4. Initial charge-discharge profiles of Cu||NCM811 pouch cells using different electrolytes and areal capacities. (a) Initial charge-discharge profiles of Cu||NCM811 pouch cells using CME with low and high areal capacities. For the battery with a high areal capacity of 5.6 mAh cm^{-2}, short circuit occurred even during the first charging process. (b) Initial charge-discharge profiles of Cu||NCM811 pouch cells (5.6 mAh cm^{-2}) using advanced electrolytes of AFE, LHCE, HCDE, and BAFF. (c) Comparison of lithium nucleation overpotentials in (b).

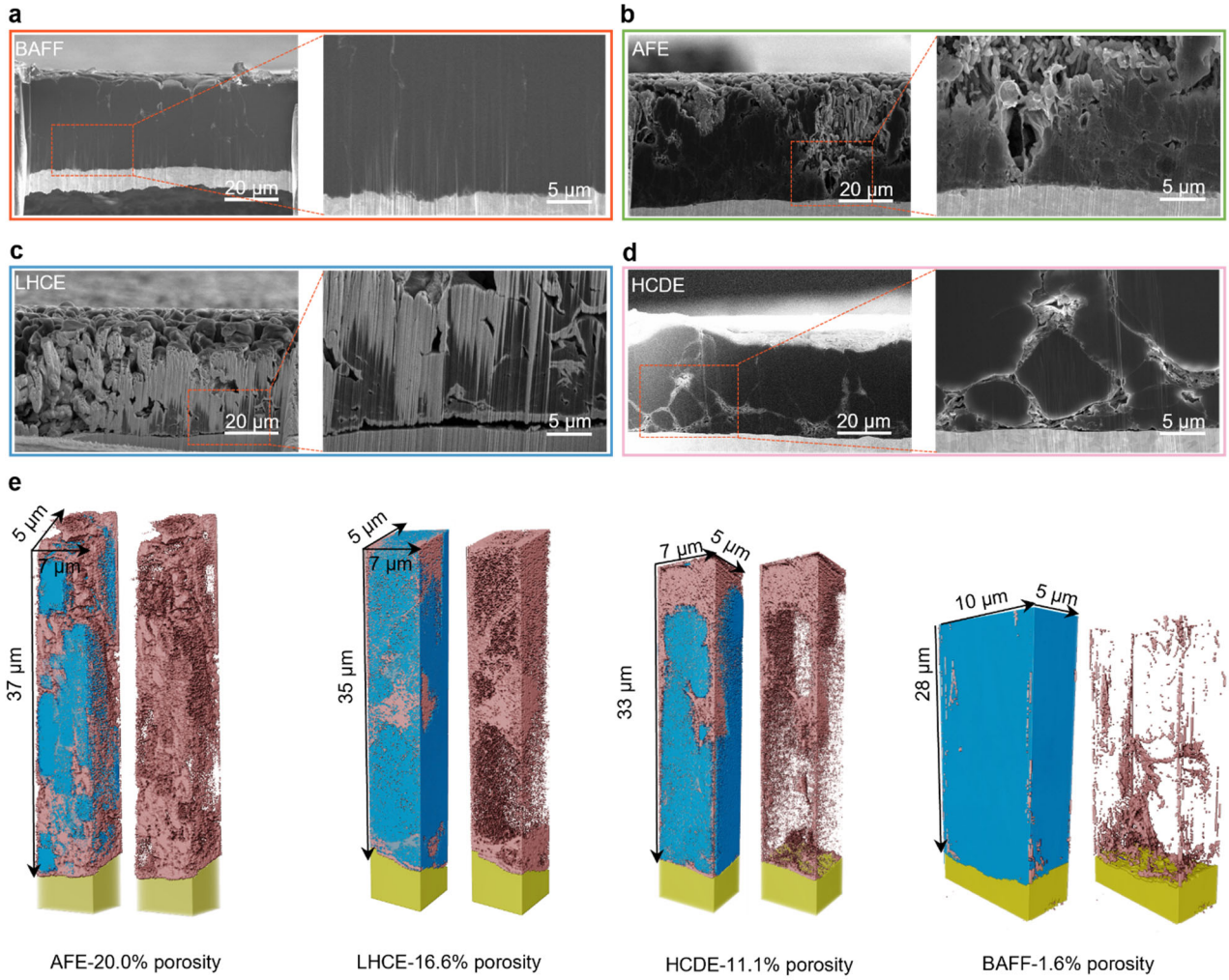

Supplementary Figure 5. Cross-section and 3D-reconstruction views of 5th deposited Li collected at 4.4 V from Cu||NCM811 pouch cells (5.6 mAh cm^{-2}) using different electrolytes. (a-d) Cryo-FIB-SEM images: (a) BAFF, (b) AFE, (c) LHCE and (d) HCDE. (e) 3D reconstruction models contrast voids (in brown) and bulk Li metal (in blue) of the deposited Li for the above four electrolytes.

The BAFF electrolyte realized the densest deposition of lithium metal with the lowest porosity as compared to the three reference electrolytes.

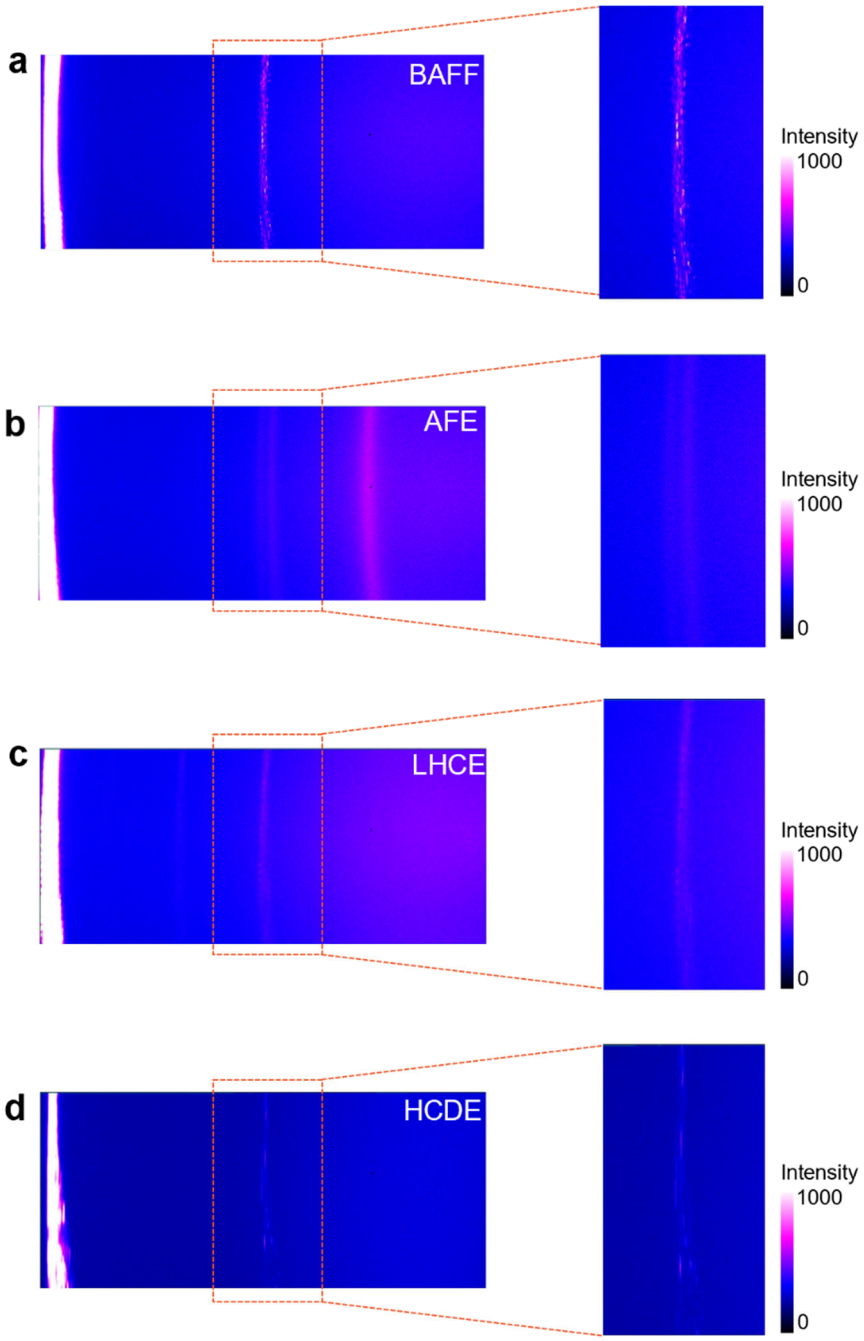

Supplementary Figure 6. 2D GIXD analysis of 5th deposited Li collected at 4.4 V from Cu||NCM811 pouch cells (5.6 mAh cm^{-2}) using different electrolytes: (a) BAFF, (b) AFE, (c) LHCE, and (d) HCDE.

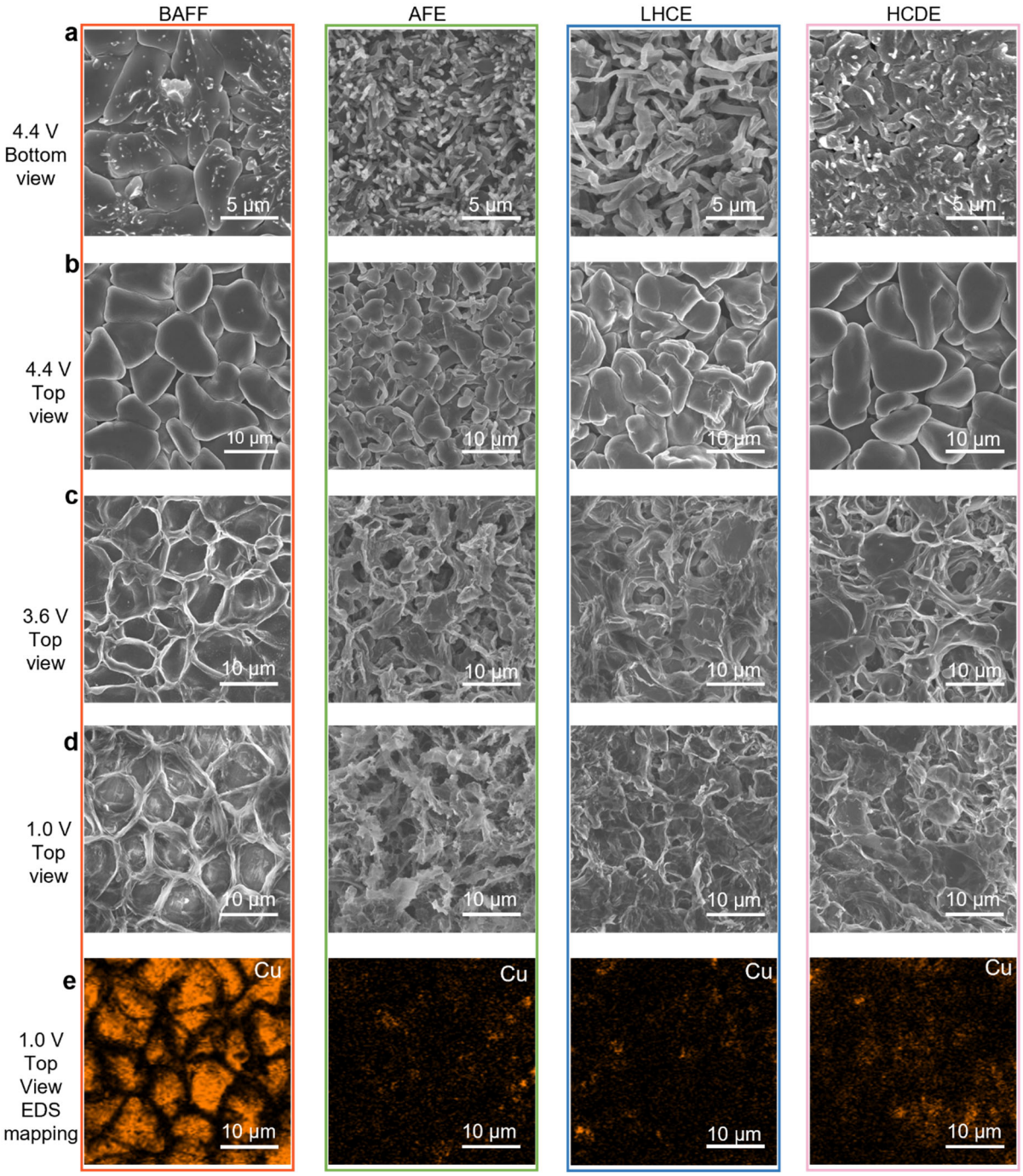

Supplementary Figure 7. Morphology evolution of 1st deposited/dissolved Li in Cu||NCM811 pouch cells (5.6 mAh cm^{-2}) using different electrolytes. (a,b) SEM images of 1st deposited Li collected at 4.4 V: (a) bottom view; (b) top view. (c,d) Top-view SEM images of 1st dissolved Li collected at (c) 3.6 V and (d) 1.0 V. (e) Cu EDS mapping of (d).

For the three reference electrolytes, a mass of lithium mosses can be observed from the bottom view; the lithium dissolution follows a 3D manner, leading to the formation of thick porous SEI, beneath which the Cu substrate cannot be seen. By contrast, for BAFF, few lithium moss can be found from the bottom view; the lithium dissolution follows a 2D manner, leading to the formation of a unique thin mesh-film-structure SEI, beneath which the Cu substrate can be clearly seen.

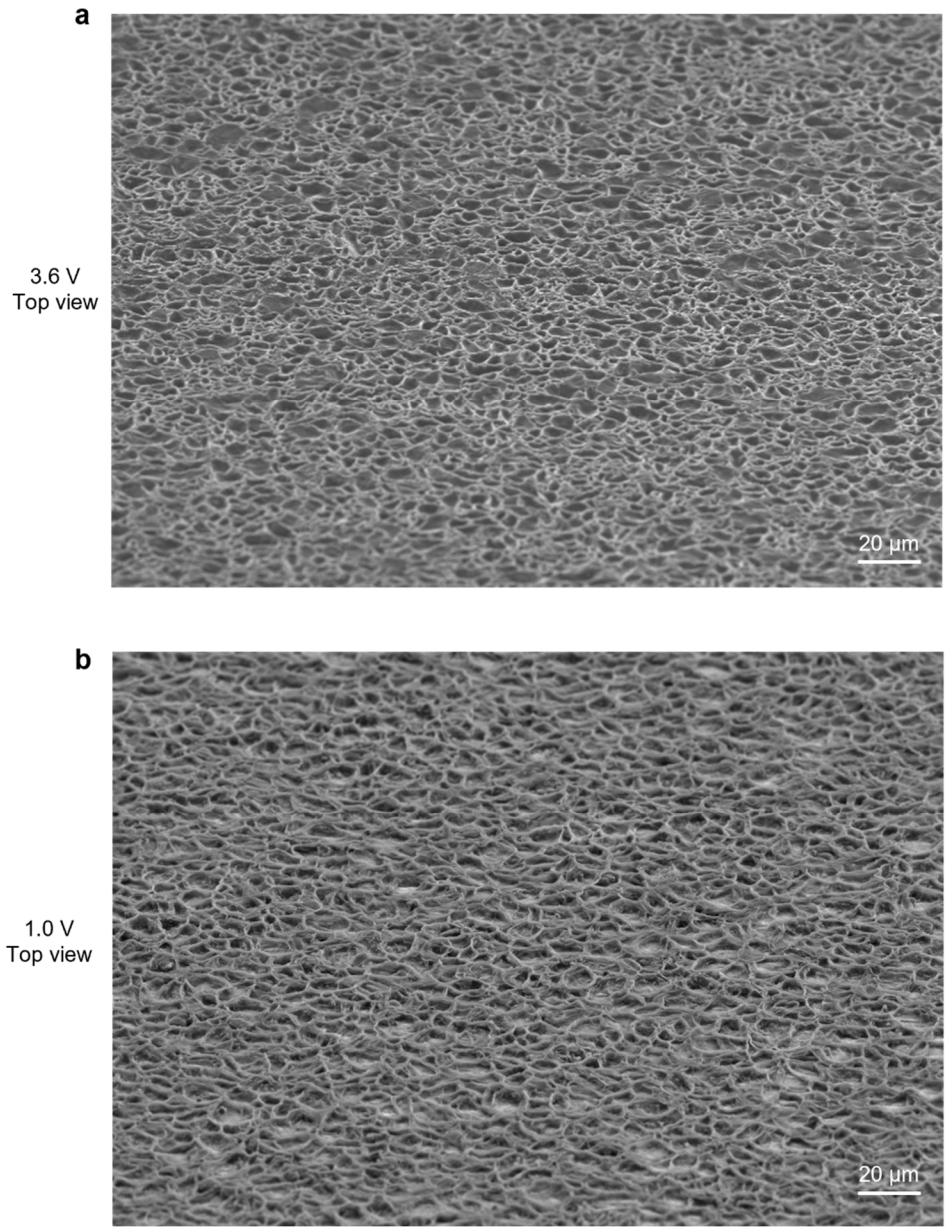

Supplementary Figure 8. Oblique angle large-view SEM images of 1st dissolved Li in BAFF: (a) 1st discharge at 3.6 V and (b) 1st discharge at 1.0 V.

The large-view SEM images clearly show that, every lithium grain has a “hemispherical pit” on the surface, demonstrating a synchronous dissolution process in BAFF, following a typical 2D manner. After full lithium dissolution at 1.0 V, a high-quality mesh-film-structured SEI appeared on the Cu surface, indicating a self-adaptive process of SEI upon the volume shrinkage of lithium grains.

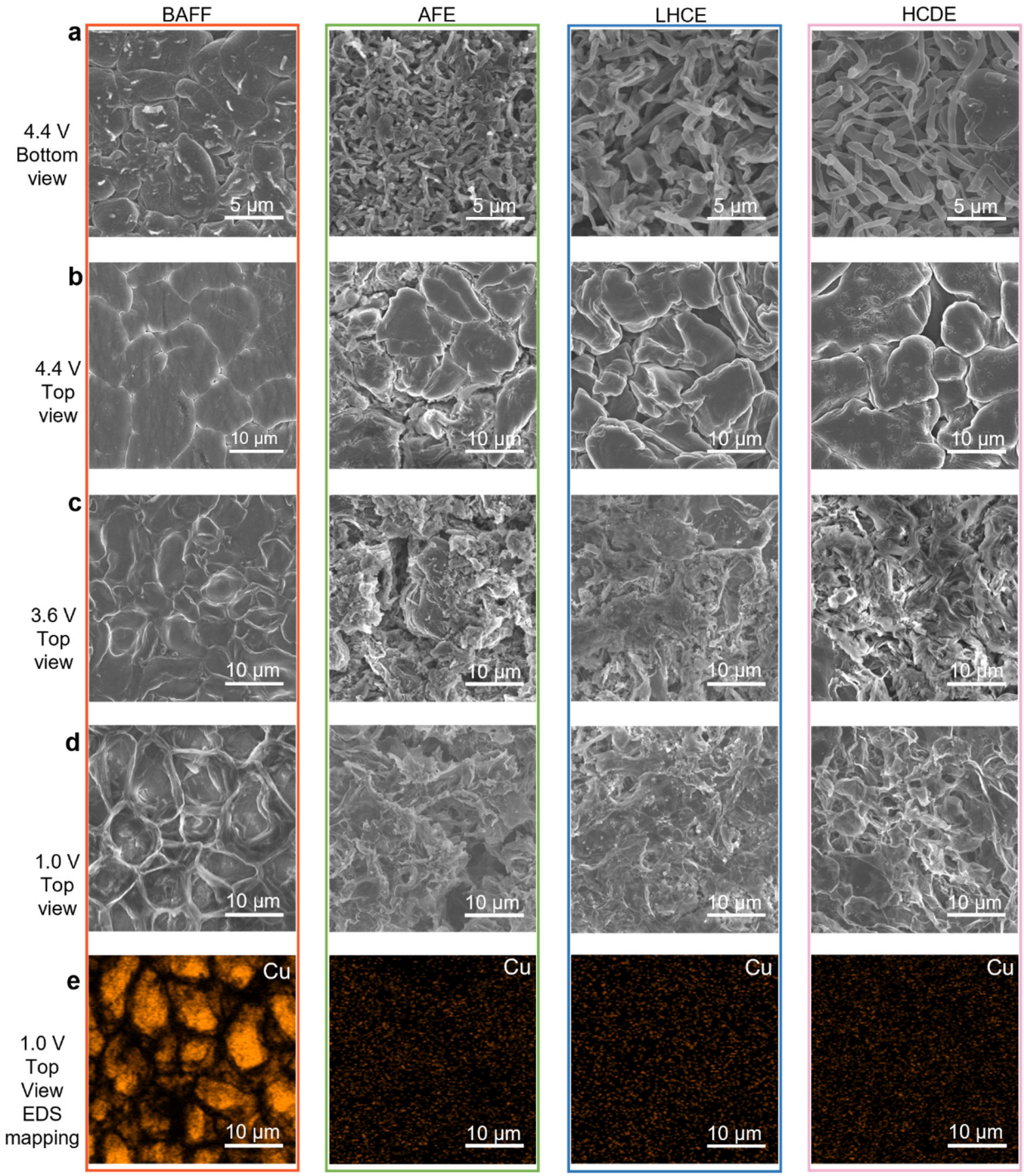

Supplementary Figure 9. Morphology evolution of 5th deposited/dissolved Li in Cu||NCM811 pouch cells (5.6 mAh cm^{-2}) using different electrolytes. (a,b) SEM images of 5th deposited Li collected at 4.4 V: (a) bottom view; (b) top view. (c,d) Top-view SEM images of 5th dissolved Li collected at (c) 3.6 V and (d) 1.0 V. (e) Cu EDS mapping of (d).

For the reference electrolytes, the lithium morphologies underwent a dynamic change and continuous deterioration during cycling. By contrast, for BAFF, the evolved mesh-film-structure SEI remained stable during cycling. Thus, this BAFF-derived SEI with excellent self-adaption to large volume change shows the capability to overcome the inherent structural instability for the host-free lithium metal electrode.

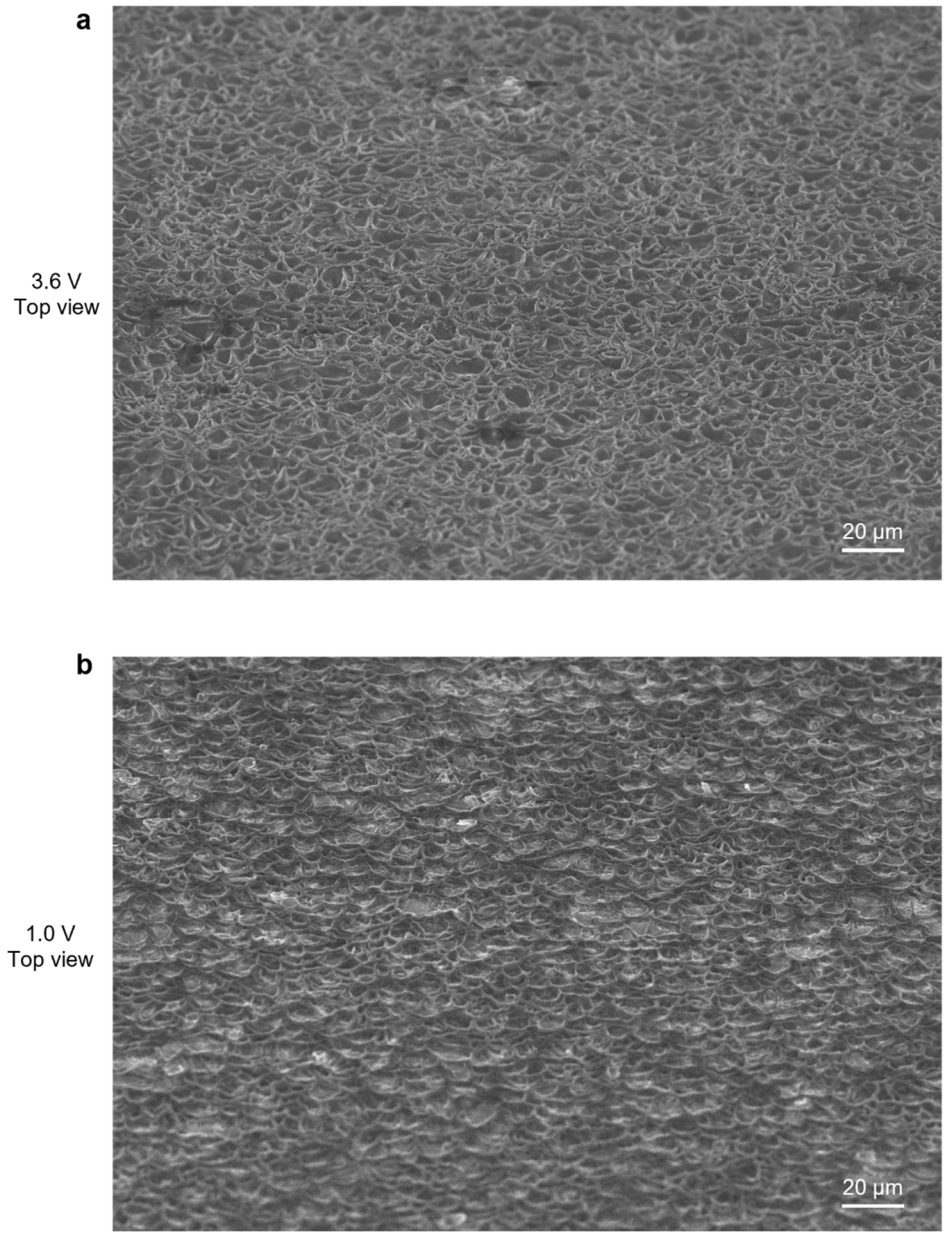

Supplementary Figure 10. Oblique angle large-view SEM images of 5th dissolved Li in BAFF: (a) 1st discharge at 3.6 V and (b) 1st discharge at 1.0 V.

The large-view SEM images firmly confirm that the BAFF-derived self-adaptive SEI keeps stable and enables reversible 2D lithium deposition/dissolution of 5.6 mAh cm^{-2} during cycling.

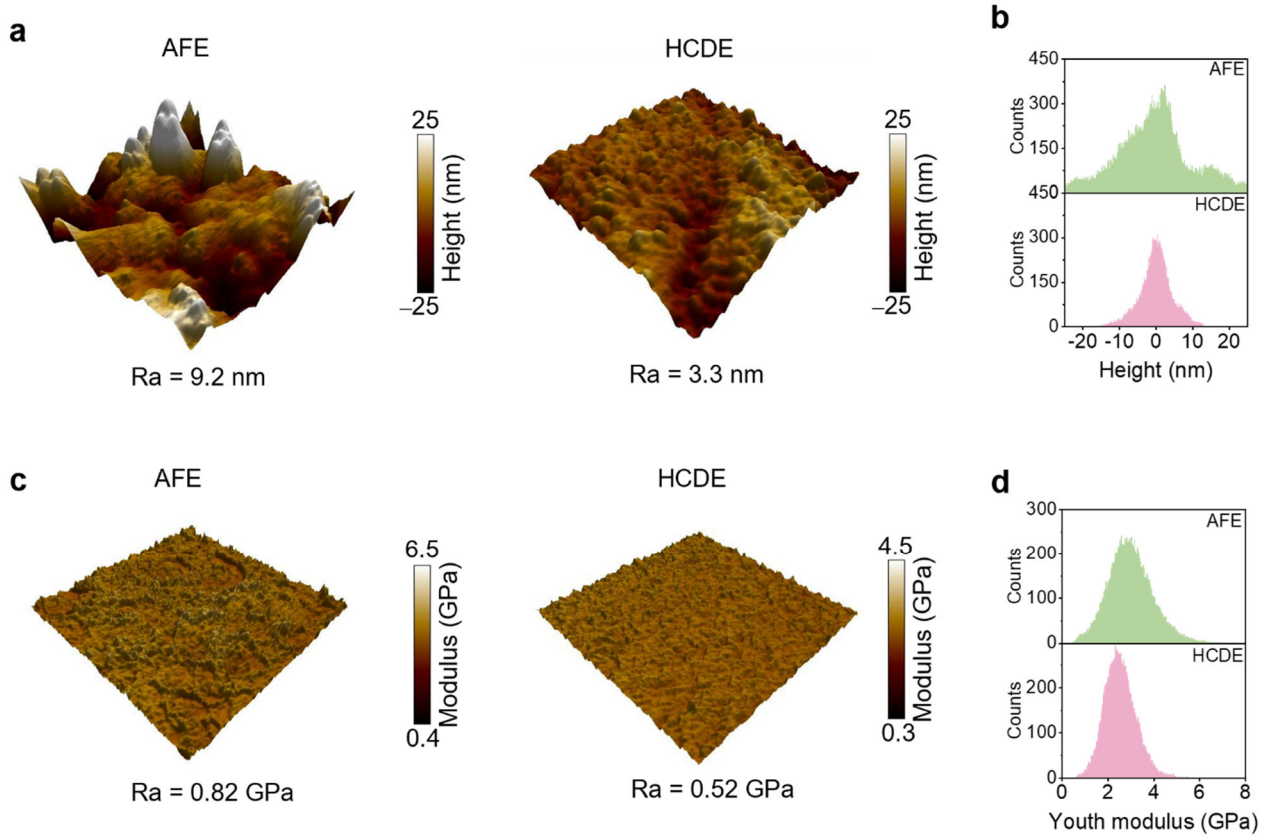

Supplementary Figure 11. **AFM results of 5th deposited Li in AFE and HCDE.** (a) The height images and (b) their distribution. (c) The Young's modulus mapping and (d) their distribution.

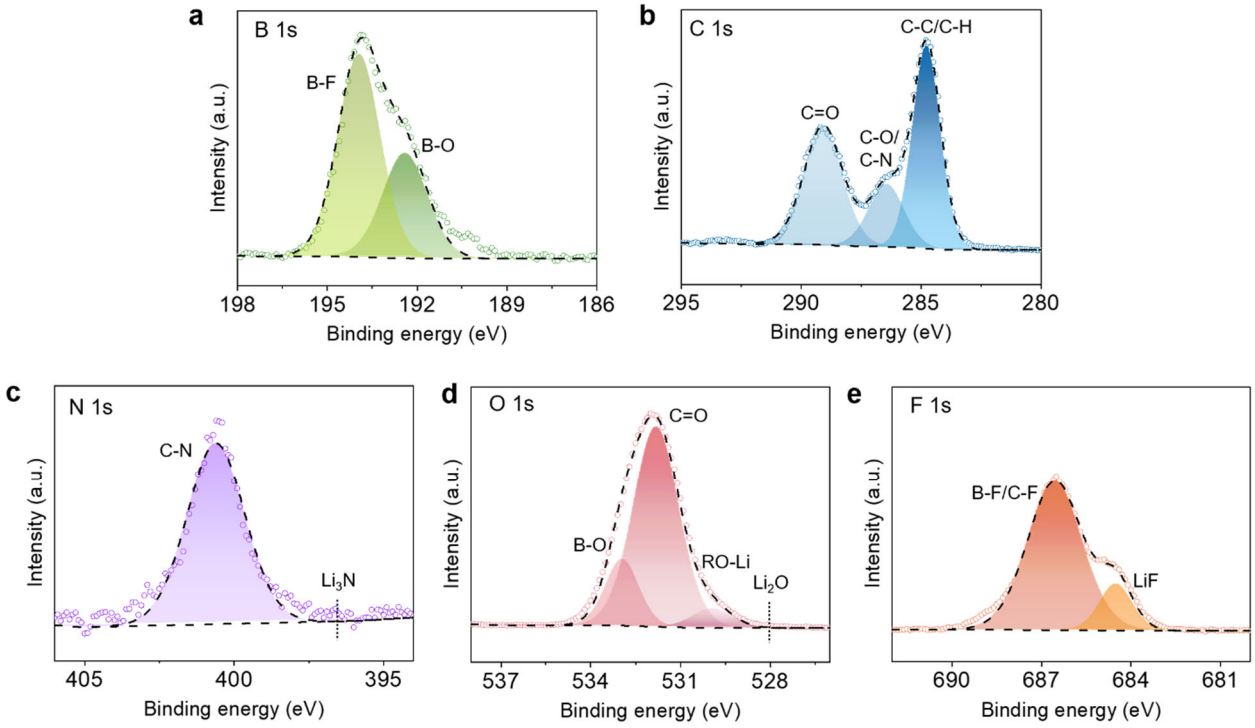

Supplementary Figure 12. **XPS spectra of BAFF-derived SEI.** (a) B 1s, (b) C 1s, (c) N 1s, (d) O 1s and (e) F 1s spectra. Only a small amount of LiF and almost absence of Li_2O and Li_3N can be observed in the BAFF-derived SEI. The sample was collected at 1.0 V from Cu||NCM811 pouch cells (5.6 mAh cm^{-2}) after five cycles. To avoid sample degradation during measurement, the applied power was operated at 100 W (10 kV, 10 mA).

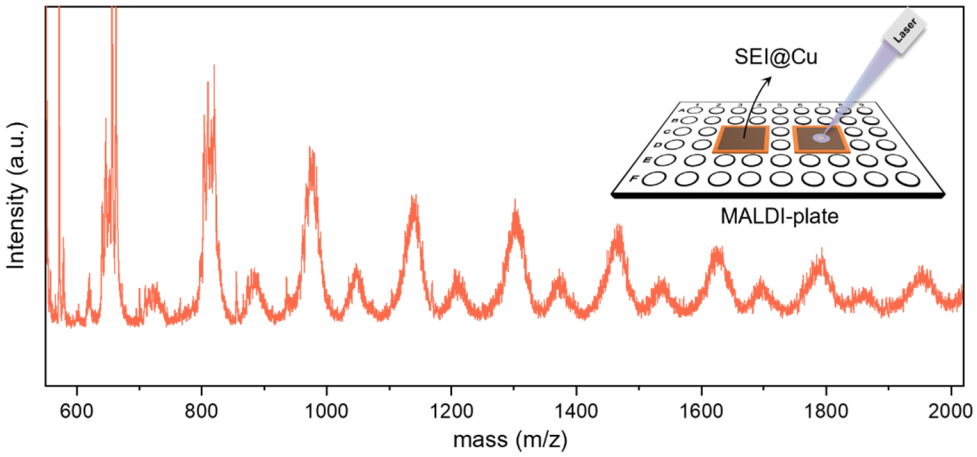

Supplementary Figure 13. **MALDI-TOF spectrum of BAFF-derived SEI.** The SEI sample was collected at 1.0 V from Cu||NCM811 pouch cell (5.6 mAh cm^{-2}) after five cycles. The result evidences the presence of polymer components with >2000 Da in the SEI. The repeat unit is 163 Da. Because the SEI sample cannot be dissolved in various high-polarity aprotic solvents, such as DMSO, PC, and NMP, and may be subject to irradiation-induced decomposition during the MALDI-TOP measurement, we deduce that the SEI could be composed of polymer components with even larger molecule weight.

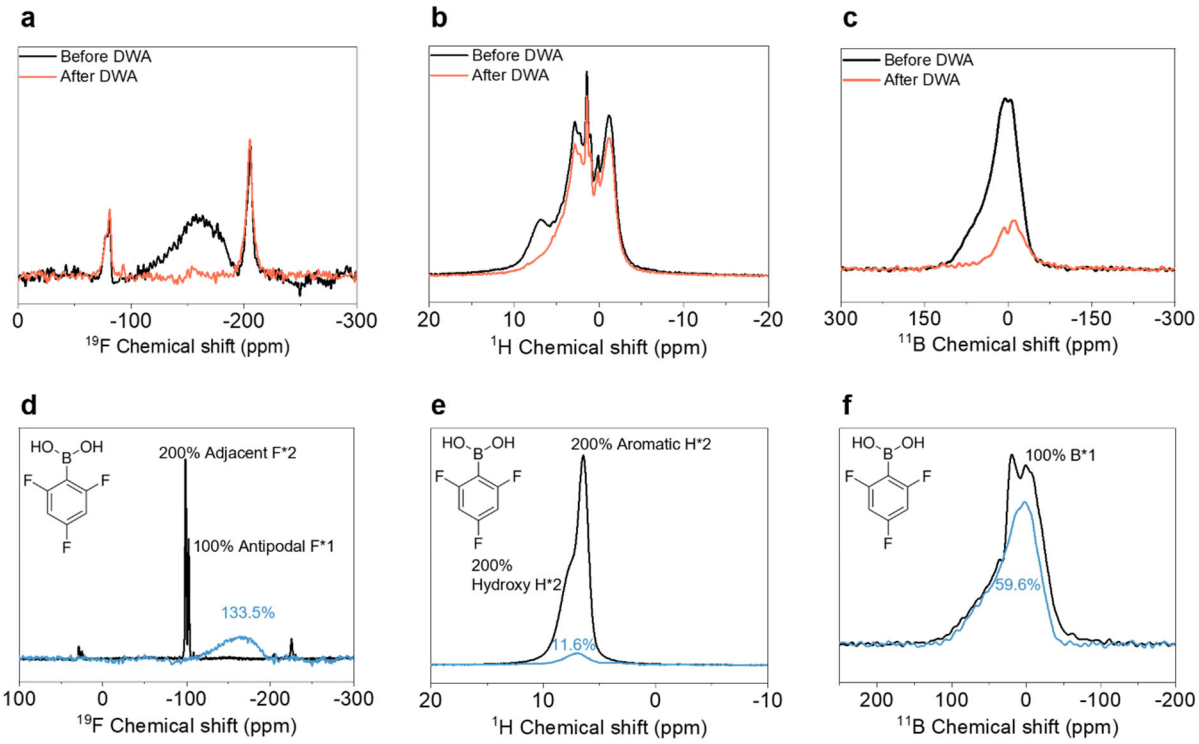

Supplementary Figure 14. **ss-NMR analysis for BAFF-derived SEI.** (a-c) ss-NMR spectra before and after dynamic weighted analysis (DWA): (a) ^{19}F, (b) ^{1}H, and (c) ^{11}B. (d-f) Quantitative analysis of the polymer components of BAFF-derived SEI via external standardization method: (d) ^{19}F, (e) ^{1}H, and (f) ^{11}B. 2,4,6-Trifluorophenylboronic acid was used as the external reference. The absolute integral ratio of ^{19}F, ^{1}H, and ^{11}B nuclei peaks in the reference is fixed (F : H : B = 300% : 200% : 100%). OH signals are neglected due to their mobility. By comparing the spectral integral of sample with the reference, the absolute integral ratio of ^{19}F, ^{1}H, and ^{11}B nuclei peaks in the polymer components can be calibrated as 133.5% : 11.6% : 59.6%. This external standardization method shows significant advantages over the internal standardization method, such as no peak overlap, no chemical reaction impact, and no need of developing a compatible reference/analyte combination.

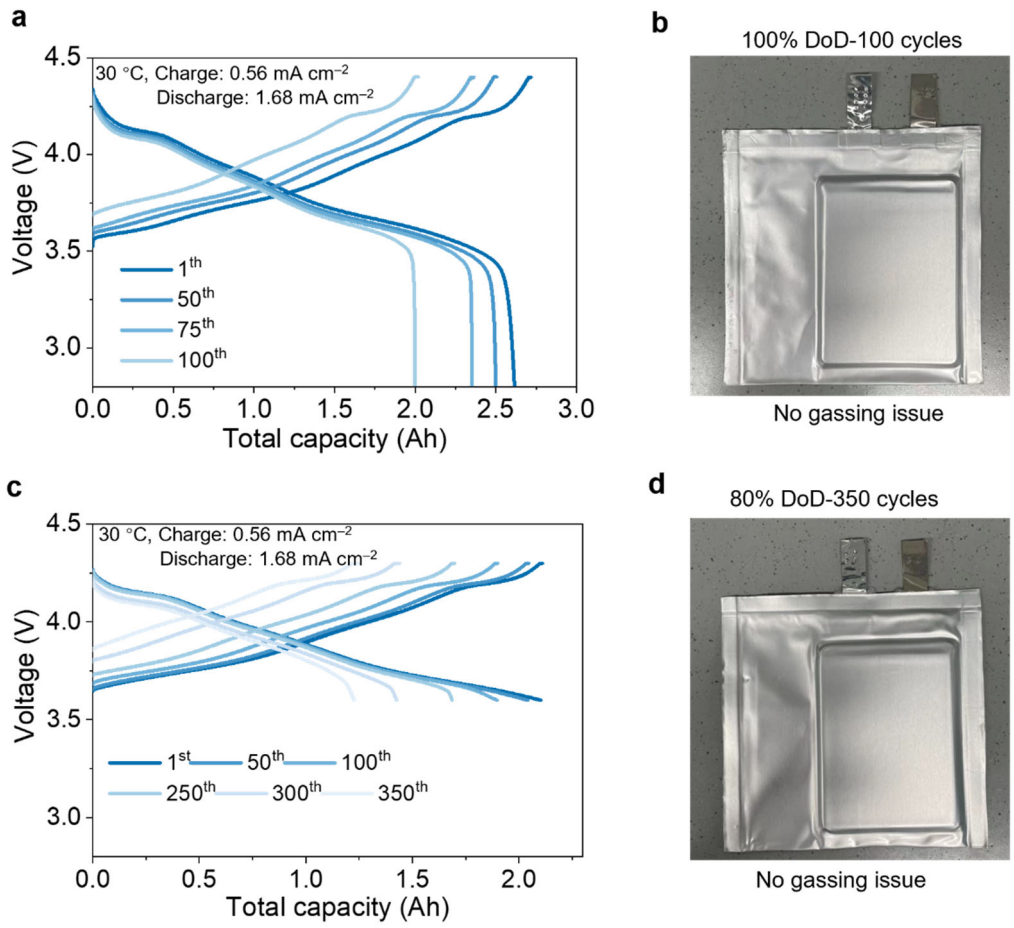

Supplementary Figure 15. Cycling performances of 2.7Ah Cu||NCM811 pouch cells using BAFF at different DoD. (a, c) Charge/discharge curves at 100% (a) and 80% DoD (c). (b, d) Optical images of the cycled Cu||NCM811 pouch cells at 100% DoD (b) and 80% DoD (d). No gas evolution was found during both initial two formation cycles and subsequent cycling process.

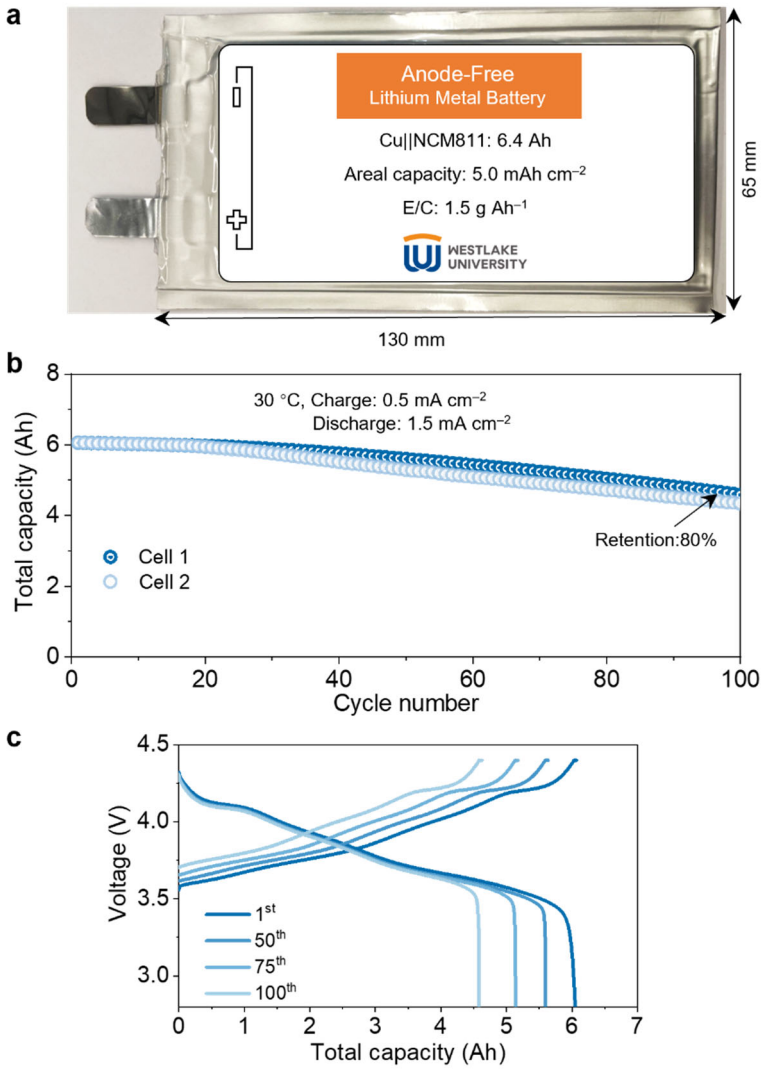

Supplementary Figure 16. Cycling performances of 6.4Ah Cu||NCM811 pouch cells using BAFF. (a) Optical image. (b) Capacity retention at 100% DoD. (c) The corresponding charge/discharge curves. The cathode areal capacity is 5.0 mAh cm^{-2}. E/C ratio is 1.5 g Ah^{-1}. The stack energy density of the pouch cells is 520 Wh kg^{-1}.

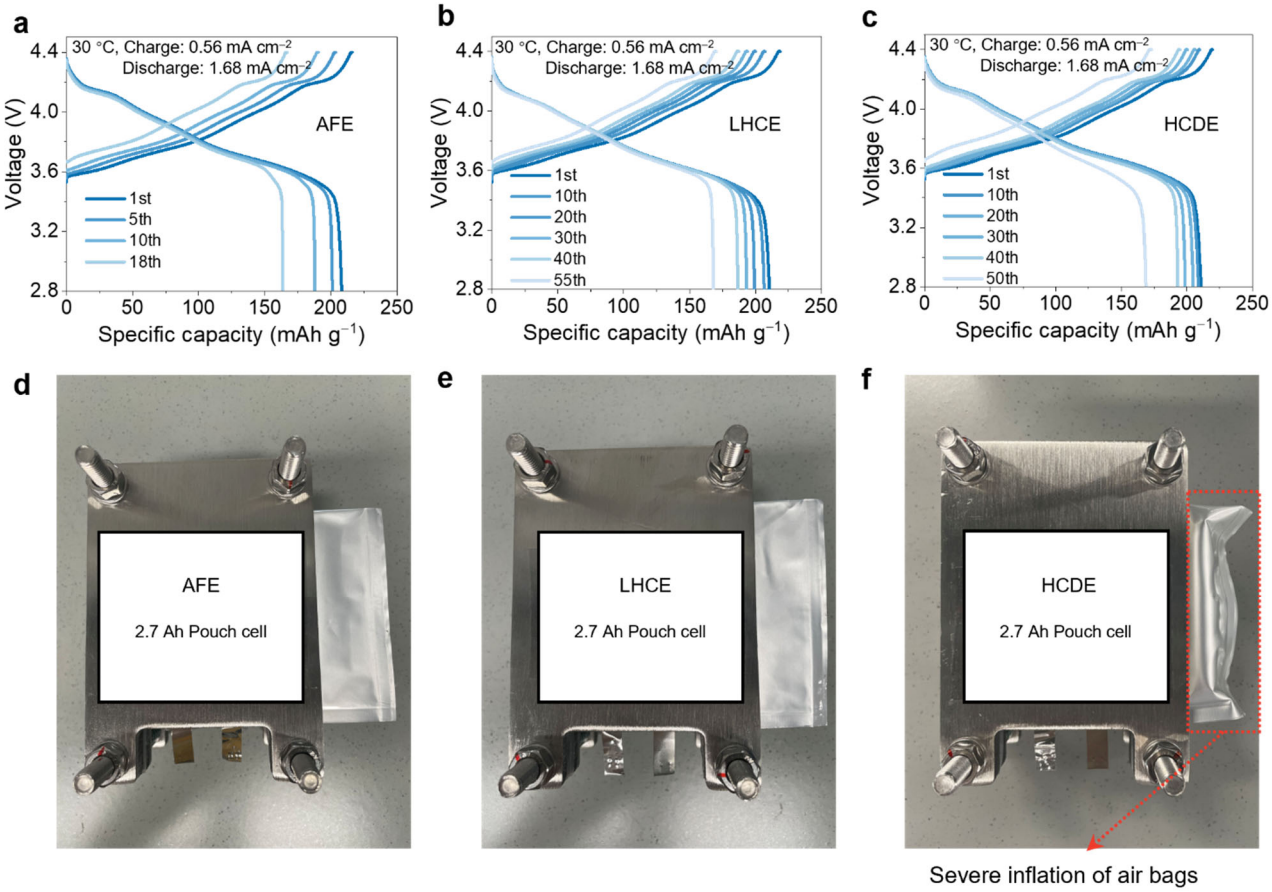

Supplementary Figure 17. Cycling performances of 2.7Ah Cu||NCM811 pouch cells using different electrolytes. (a-c) Charge/discharge curves of pouch cells: (a) AFE, (b) LHCE and (c) HCDE. (d-f) Optical images of cycled pouch cells with 80% capacity retention: (d) AFE, (e) LHCE and (f) HCDE. The pouch cell using HCDE produced a large amount of gas during cycling.

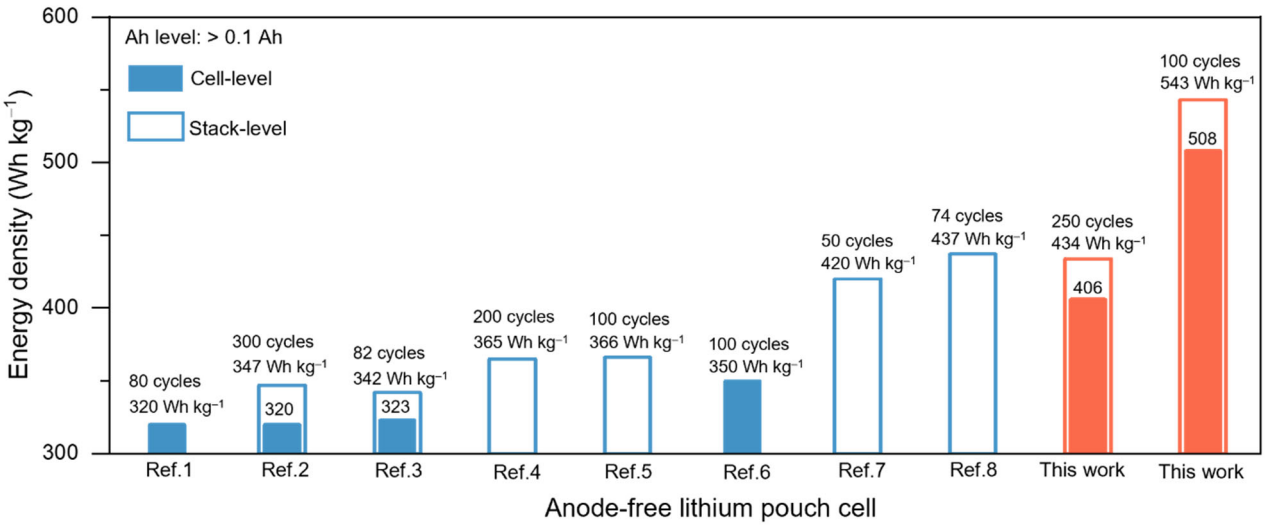

Supplementary Figure 18. Comparison of state-of-the-art Ah-level high-energy-density anode-free Li pouch cells in literature and this work. Detailed battery information is listed in Table S8.

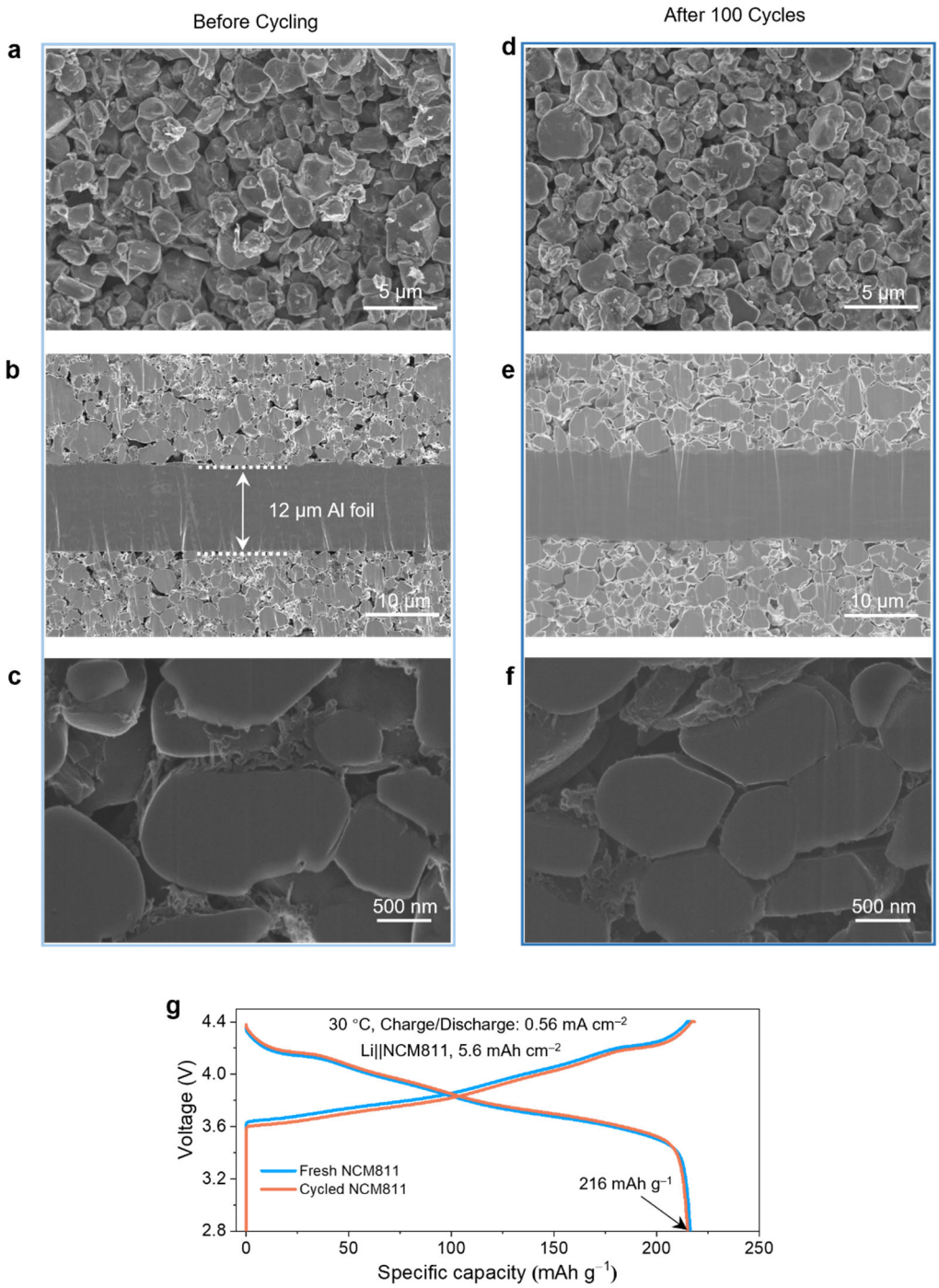

Supplementary Figure 19. Comparison in morphology and reversible capacity of NCM811 cathode (5.6 mAh cm^{-2}) before and after cycling. (a-c) Morphology of fresh NCM811 cathode: (a) Top-view SEM image; (b) Cross-sectional view SEM images; (c) Enlarged image in (b). (d-f) Morphology of the cycled NCM811 cathode: (d) Top-view SEM image; (e) Cross-sectional view SEM images; (f) Enlarged image in (e). (g) Charge-discharge curves of fresh NCM811 and cycled NCM811 in BAFF. The cycled NCM811 cathode was retrieved from a Cu||NCM811 pouch cell after 100 cycles at 100% DoD and re-assembled in a half-cell with fresh lithium metal anode and electrolyte. No morphology change and no capacity decay can be found for the cycled cathode material.

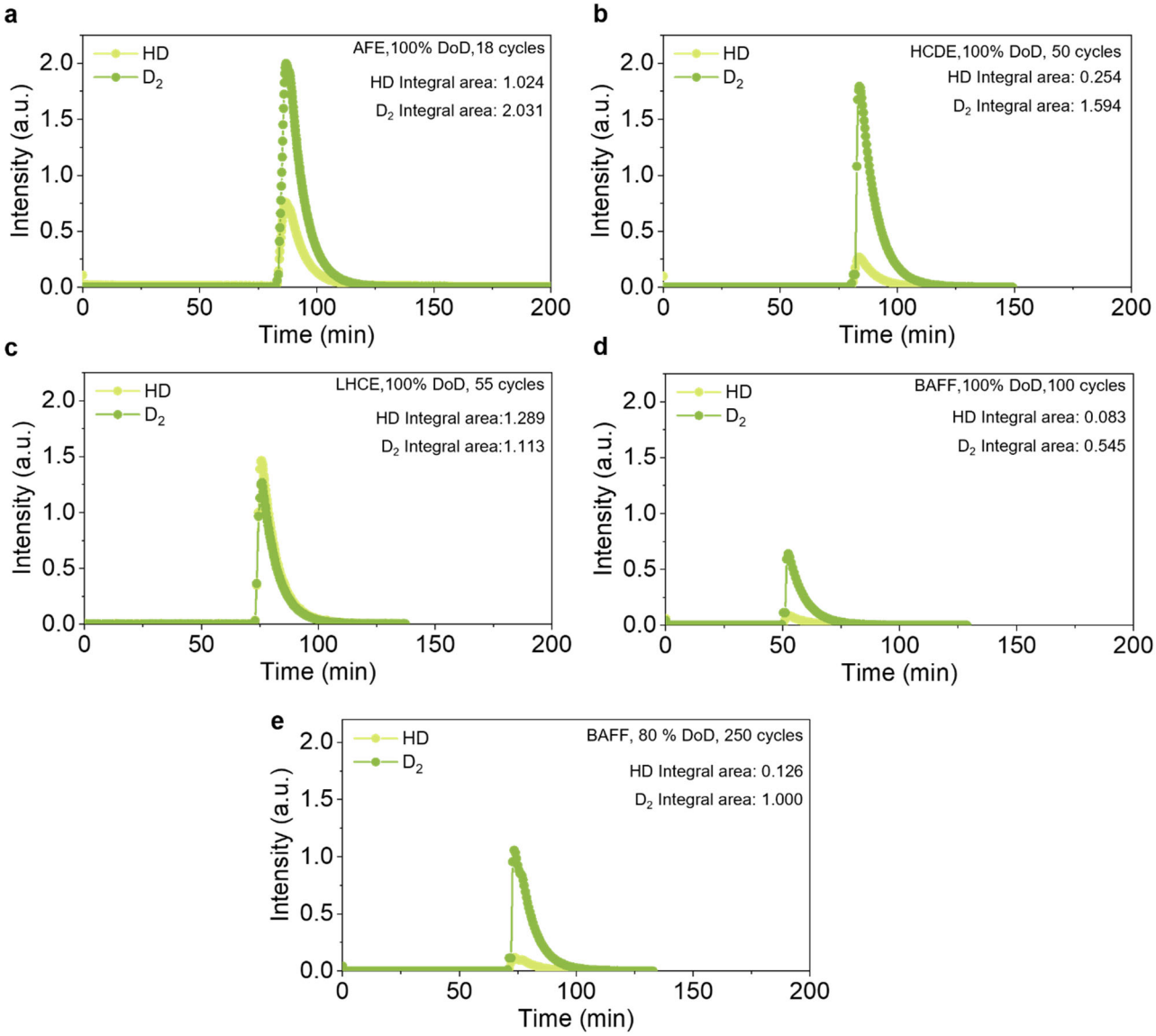

Supplementary Figure 20. **MST quantitative analysis of inactive Li metal and LiH in 2.7 Ah Cu||NCM811 pouch cells with 80% capacity retention.** (a) With AFE after 18 cycles at 100% DoD, (b) HCDE-100% DoD, (c) LHCE-100% DoD, (d) BAFF-100% DoD, and (e) BAFF-80% DoD.

Supplementary tables

Supplementary Table 1 Battery price per kWh of LIBs, LMBs and AFLMBs.

Battery type	Battery		Price (USD kWh^{-1})	Price (CNY kWh^{-1})
Graphite based-LIB	Graphite||LFP	160 Wh kg^{-1}	86.75	627
	Graphite||NCM523	240 Wh kg^{-1}	110.68	800
	Graphite||NCM622	260 Wh kg^{-1}	146.65	1060
	Graphite||NCM811	280 Wh kg^{-1}	168.79	1220
Si/C based-LIB	Si/C||LFP	200 Wh kg^{-1}	98.23	710
	Si/C||NCM523	275 Wh kg^{-1}	125.90	910
	Si/C||NCM622	290 Wh kg^{-1}	166.02	1200
	Si/C||NCM811	320 Wh kg^{-1}	192.31	1390
	Si/C||NCM811	360 Wh kg^{-1}	332.05	2400
LMB	Lithium||LFP	245 Wh kg^{-1}	180.43	1304
	Lithium||NCM523	330 Wh kg^{-1}	200.33	1448
	Lithium||NCM622	350 Wh kg^{-1}	245.65	1776
	Lithium||NCM811	390 Wh kg^{-1}	275.13	1989
	Lithium||NCM811	450 Wh kg^{-1}	393.28	2843
AFLMB	Cu||LFP	305 Wh kg^{-1}	68.53	495
	Cu||NCM523	400 Wh kg^{-1}	91.31	660
	Cu||NCM622	450 Wh kg^{-1}	122.46	885
	Cu||NCM811	520 Wh kg^{-1}	141.78	1025

Note: The price information of commercial Graphite-based and Si/C-based LIBs is based on the Chinese market from 2022 to 2024. The price of LMBs was estimated on that of commercial Graphite-based LIBs by replacing the graphite materials with ultra-thin Li foils. The price of AFLMBs was estimated on that of commercial Graphite-based LIBs by subtracting the cost of the graphite materials. The exchange rate between US Dollar (USD) and Chinese Yuan (CNY) is set to be 7.23.

Supplementary Table 2 Commercially available components for Li-ion batteries.

Components	Specification	Areal density (mg cm^{-2})
Al foil	Al–12 μm	3.24
	Al–14 μm	3.78
	Al–15 μm	4.05
	Al–16 μm	4.32
Cu foil	Cu–4 μm	3.60
	Cu–6 μm	5.38
	Cu–8 μm	7.15
	Cu–12 μm	10.73
Separator	Separator–9 μm	0.485
	Separator–12 μm	0.646
	Separator–16 μm	0.861
	Separator–18 μm	0.969
	Separator–20 μm	1.080
Al plastic film	Al-plastic-film–88 μm	14.30
	Al-plastic-film–113 μm	17.97
	Al-plastic-film–144 μm	20.38
	Al-plastic-film–152 μm	21.51
Ni tabs	Ni–80 μm	71.2
	Ni–100 μm	89.02
	Ni–150 μm	133.53
Al tabs	Al–80 μm	21.62
	Al–100 μm	27.02
	Al–150 μm	40.53
	Al–200 μm	54.04

Supplementary Table 3 Correlation of cell parameters and energy density for Graphite||NCM Li-ion pouch cells.

Cell properties	Cell parameters	Symbols	Corresponding calculations
LIB structure	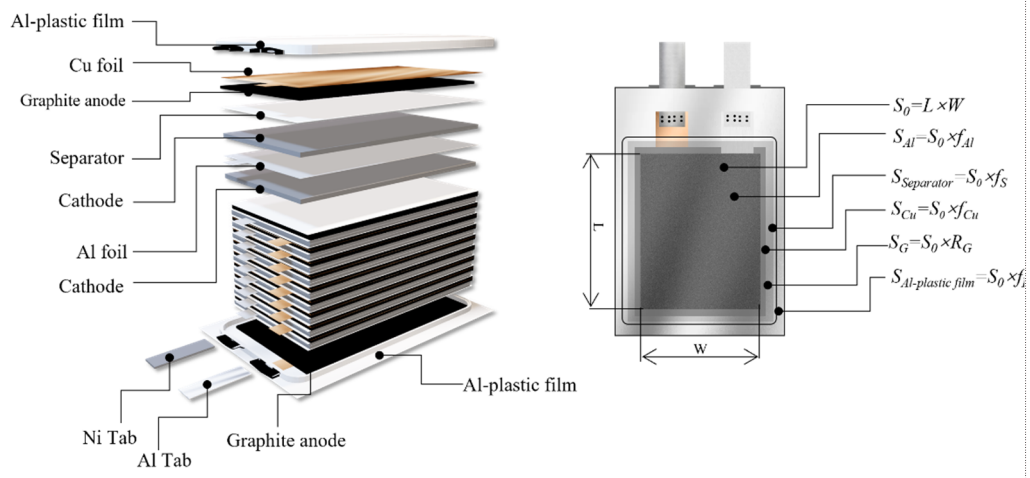		
Cathode (M_c/g)	Specific capacity (mAh g^{-1})	C_0	$M_c=\frac{n\times S_0\times C_c\times 2}{P_c\times C_0}$
	Number of layers	n	
	Area (L×W, cm^2)	S_0	
	Areal capacity (mAh cm^{-2}), double coating	$2\times C_c$	
	Active material percentage (%)	P_c	
Al foil (M_{Al}/g)	Areal density (g cm^{-2})	ρ_{Al}	$M_{Al}=\rho_{Al}\times(f_{Al}\times S_0)\times n$
	Factor (f_{Al}, including the Al pole)	f_{Al}	
Cu foil (M_{Cu}/g)	Areal density (g cm^{-2})	ρ_{Cu}	$M_{Cu}=\rho_{Cu}\times(f_{Cu}\times S_0)\times(n+1)$
	Factor (including anode area redundancy and the Cu pole)	f_{Cu}	
Graphite (M_G/g)	Specific capacity (mAh g^{-1})	C_0'	$M_G=\frac{n\times R_G\times S_0\times C_c\times 2}{P_G\times C_0'}$
	Active material percentage (%)	P_G	
	N/P capacity ratio	R_G	
Separator (M_p/g)	Areal density (g cm^{-2})	ρ_S	$M_s=\rho_S\times(f_S\times S_0)\times(2n+2)$
	Factor (Z-folded separator)	f_S	
Al-plastic-film (M_p/g)	Areal density (g cm^{-2})	ρ_p	$M_p=\rho_P\times(f_P\times S_0)$
	Factor (including the Ni, Al tabs and sealing edges)	f_p	
Electrolyte (M_e/g)	E/C ratio (g Ah^{-1})	R_e	$M_e=R_e\times n\times S_0\times C_c\times 2\times 10^{-3}$
Total mass (M_T/kg)	$M_T=(M_c+M_{Al}+M_{Cu}+M_G+M_s+M_p+M_e)\times 10^{-3}$		
	$M=(\frac{2nS_0C_c}{P_cC_0}+\frac{2nR_GS_0C_c}{P_GC_0'}+\rho_{Al}f_{Al}S_0n+\rho_{Cu}f_{Cu}S_0(n+1)+\rho_Sf_SS_0(2n+2)+\rho_pf_pS_0+2nS_0C_cR_e\times 10^{-3})\times 10^{-3}$		
Average voltage (U/V)	U		
Capacity utilization (R_i)	R_i		
Total capacity (C_T/Ah)	$C_T=n\times S_0\times C_c\times 2\times 10^{-3}\times R_i$		
Gravimetric energy density (E/Wh kg^{-1})	$E=\frac{C_T\times U}{M}=\frac{2nC_cUR_i}{n\times(\frac{2C_cR_G}{P_cC_0R_C}+\frac{2R_GC_c}{P_GC_0'}+\rho_{Al}f_{Al}+\rho_{Cu}f_{Cu}+2f_S\rho_S+2C_cR_e\times 10^{-3})+\rho_Pf_P+\rho_{Cu}f_{Cu}+2\rho_Sf_S}$		
Relationship among C_c, R_e, n, and E	$C_c=\frac{-\left(\frac{\rho_Pf_P+\rho_{Cu}f_{Cu}+2\rho_Sf_S}{2n}+\frac{\rho_{Al}f_{Al}+\rho_{Cu}f_{Cu}+2\rho_Sf_S}{2}\right)}{R_e\times 10^{-3}-\frac{UR_i}{E}+\frac{1}{P_cC_0}+\frac{R_G}{P_GC_0'}}$		

For LGES E78–78 Ah pouch cell, 4.2V NCM712 cathode, 12 μm Cu foil, 18 μm separator and 144 μm Al-plastic-film are adopted.

Cell components/properties	Parameters & symbols	Values
Cathode-4.3V NCM712	Specific capacity (C_0)	190 mAh g^{-1}
	Active material percentage (P_c)	97.5%
Al foil-14 μm	Areal density (ρ_{Al})	3.78×10^{-3} g cm^{-2}
	Factor (f_{Al}, including the Al pole)	1.06
Cu foil-12 μm	Areal density (ρ_{Cu})	10.73×10^{-3} g cm^{-2}
	Factor (f_{Cu}, including anode area redundancy and the Cu pole)	1.15
Graphite	Specific capacity (C_0')	360 mAh g^{-1}
	Active material percentage (P_G)	95.5%
	N/P capacity ratio (R_G)	1.04
Separator-18 μm	Areal density (ρ_S)	0.969×10^{-3} g cm^{-2}
	Factor (f_S, Z-folded separator)	1.08
Al-plastic-film-144 μm	Areal density (ρ_P)	20.38×10^{-3} g cm^{-2}
	Factor (f_P, including the Ni, Al tabs and sealing edges)	4.09
Average voltage	U	3.70 V
Capacity utilization	R_i	91.8 %
Relationship among C_c, R_e, n, and E	$C_c=\frac{-\left(\frac{48.89335}{n}+9.21965\right)}{R_e-\frac{3396.6}{E}+8.423}$	
Relationship among C_c, R_e and n (E = 268 Wh kg^{-1})	$C_c=\frac{-\left(\frac{48.89335}{n}+9.21965\right)}{R_e-4.2509}$	

When E=268 Wh kg^{-1}, n=18, R_e=1.9 g Ah^{-1}, we can obtain C_c=5.08 mAh cm^{-2}.
This calculated result closely approximates the actual value (5.02 mAh cm^{-2}) of the LGES E78 pouch cell[9].

For Li-FUN Technology 402035–0.24 Ah pouch cell, 4.3V NCM523 cathode, 8 μm Cu foil, 16 μm separator and 113 μm Al-plastic-film are adopted.

Cell components/properties	Parameters & symbols	Values
Cathode-4.3V NCM523	Specific capacity (C_0)	175 mAh g^{-1}
	Active material percentage (P_c)	94.0%
Al foil-15 μm	Areal density (ρ_{Al})	4.05×10^{-3} g cm^{-2}
	Factor (f_{Al}, including the Al pole)	1.06
Cu foil-8 μm	Areal density (ρ_{Cu})	7.15×10^{-3} g cm^{-2}
	Factor (f_{Cu}, including anode area redundancy and the Cu pole)	1.15
Graphite	Specific capacity (C_0')	350 mAh g^{-1}
	Active material percentage (P_G)	95.4%
	N/P capacity ratio (R_G)	1.1
Separator-16 μm	Areal density (ρ_S)	0.861×10^{-3} g cm^{-2}
	Factor (f_S, Z-folded separator)	1.08
Al-plastic-film-88 μm	Areal density (ρ_P)	14.3×10^{-3} g cm^{-2}
	Factor (f_P, including the Ni, Al tabs and sealing edges)	4.09
Average voltage	U	3.75 V
Capacity utilization	R_i	90.0%
Relationship among C_c, R_e, n, and E	$C_c=\frac{-\left(\frac{34.2835}{n}+7.1865\right)}{R_e-\frac{3375}{E}+9.3734}$	
Relationship among C_c, R_e and n (E = 200 Wh kg^{-1})	$C_c=\frac{-\left(\frac{34.2835}{n}+7.1865\right)}{R_e-7.5016}$	

When E=200 Wh kg^{-1}, n=6, R_e=3.8 g Ah^{-1}, we can obtain C_c=3.48 mAh cm^{-2}.
This calculated result closely approximates the actual value (3.5 mAh cm^{-2}) of the Li-FUN Technology 402035 pouch cell[10].

When the battery adopts 4.4V NCM811, 4 μm Cu foil, 12 μm separator and 88 μm Al-plastic-film,

Cell components/properties	Parameters & symbols	Values
Cathode-4.4V NCM811	Specific capacity (C_0)	216 mAh g^{-1}
	Active material percentage (P_c)	97.5%
Al foil-12 μm	Areal density (ρ_{Al})	3.24×10^{-3} g cm^{-2}
	Factor (f_{Al}, including the Al pole)	1.06
Cu foil-4 μm	Areal density (ρ_{Cu})	3.60×10^{-3} g cm^{-2}
	Factor (f_{Cu}, including anode area redundancy and the Cu pole)	1.15
Graphite	Specific capacity (C_0')	356 mAh g^{-1}
	Active material percentage (P_G)	95.7%
	N/P capacity ratio (R_G)	1.1
Separator-12 μm	Areal density (ρ_S)	0.646×10^{-3} g cm^{-2}
	Factor (f_S, Z-folded separator)	1.08
Al-plastic-film-88 μm	Areal density (ρ_P)	14.30×10^{-3} g cm^{-2}
	Factor (f_P, including the Ni, Al tabs and sealing edges)	4.09
Average voltage	U	3.70 V
Capacity utilization	R_i	90%
Relationship among C_c, R_e, n, and E	$C_c=\frac{-\left(\frac{32.011}{n}+4.4849\right)}{R_e-\frac{3330}{E}+7.977}$	
Relationship among R_e, n, and E (C_c=5.6 mAh cm^{-2})	$5.6=\frac{-\left(\frac{32.011}{n}+4.4849\right)}{R_e-\frac{3330}{E}+7.977}$	

When C_c=5.6 mAh cm^{-2}, n=10, R_e=2.5 g Ah^{-1}, we can obtain E=280 Wh kg^{-1}.
When C_c=5.6 mAh cm^{-2}, n=10, R_e=2.0 g Ah^{-1}, we can obtain E=293 Wh kg^{-1}.
When C_c=5.6 mAh cm^{-2}, n=10, R_e=1.5 g Ah^{-1}, we can obtain E=307 Wh kg^{-1}.

Supplementary Table 4 Correlation of cell parameters and energy density for Cu||NCM anode-free lithium pouch cells.

Cell properties	Cell parameters	Symbols	Corresponding calculations
AFLMB structure	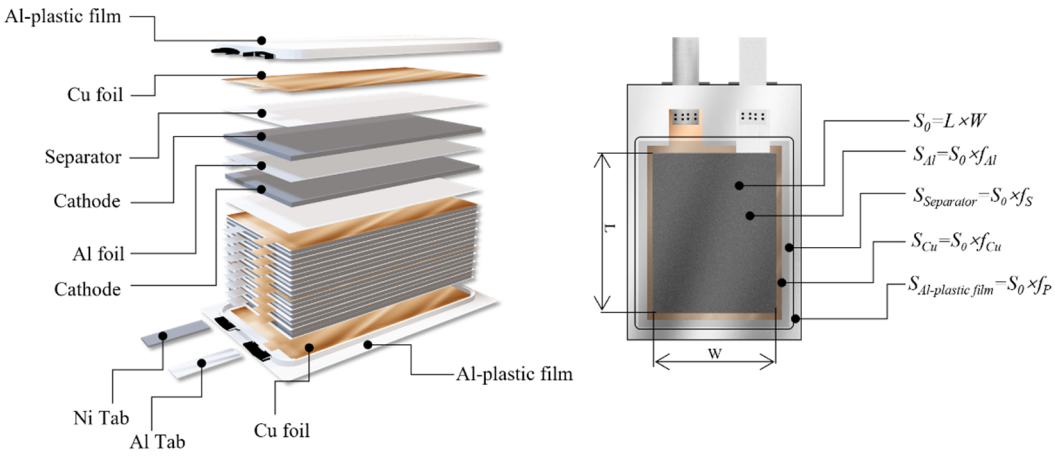		
Cathode (M_c/g)	Specific capacity (mAh g^{-1})	C_0	$M_c=\frac{n\times S_0\times C_c\times 2}{P_c\times C_0}$
	Number of layers	n	
	Area (L×W, cm^2)	S_0	
	Areal capacity (mAh cm^{-2}), double coating	$2\times C_c$	
	Active material percentage (%)	P_c	
Al foil (M_{Al}/g)	Areal density (g cm^{-2})	ρ_{Al}	$M_{Al}=\rho_{Al}\times(f_{Al}\times S_0)\times n$
	Factor (including the Al pole)	f_{Al}	
Cu foil (M_{Cu}/g)	Areal density (g cm^{-2})	ρ_{Cu}	$M_{Cu}=\rho_{Cu}\times(f_{Cu}\times S_0)\times(n+1)$
	Factor (including area redundancy and the Cu pole)	f_{Cu}	
Separator (M_s/g)	Areal density (g cm^{-2})	ρ_S	$M_s=\rho_S\times(f_S\times S_0)\times(2n+2)$
	Factor (Z-folded separator)	f_S	
Al-plastic-film (M_p/g)	Areal density (g cm^{-2})	ρ_p	$M_p=\rho_P\times(f_P\times S_0)$
	Factor (including the Ni, Al tabs and sealing edges)	f_p	
Electrolyte (M_e/g)	E/C ratio (g Ah^{-1})	R_e	$M_e=R_e\times n\times S_0\times C_c\times 2\times 10^{-3}$
Total mass (M_T/kg)	$M_T=(M_c+M_{Al}+M_{Cu}+M_s+M_p+M_e)\times 10^{-3}$		
	$M=(\frac{2nS_0C_c}{P_cC_0}+\rho_{Al}f_{Al}S_0n+\rho_{Cu}f_{Cu}S_0(n+1)+\rho_Sf_SS_0(2n+2)+\rho_Pf_PS_0+2nS_0C_cR_e\times 10^{-3})\times 10^{-3}$		
Average voltage (U/V)	U		
Capacity utilization	R_i		
Total capacity (C_T/Ah)	$C_T=n\times S_0\times C_c\times 2\times 10^{-3}\times R_i$		
Gravimetric energy density (E/Wh kg^{-1})	$E=\frac{C_T\times U}{M}=\frac{2nC_cUR_i}{n\times(\frac{2C_c}{P_cC_0}+\rho_{Al}f_{Al}+\rho_{Cu}f_{Cu}+2\rho_Sf_S+2C_cR_e\times 10^{-3})+\rho_Pf_P+\rho_{Cu}f_{Cu}+2\rho_Sf_S}$		
Relationship among C_c, R_e, n, and E	$C_c=\frac{-\left(\frac{\rho_Pf_P+\rho_{Cu}f_{Cu}+2\rho_Sf_S}{2n}+\frac{\rho_{Al}f_{Al}+\rho_{Cu}f_{Cu}+2\rho_Sf_S}{2}\right)}{R_e\times 10^{-3}-\frac{UR_i}{E}+\frac{1}{P_cC_0}}$		

When the battery adopts 4.4V NCM811, 4 μm Cu foil and 88 μm Al-plastic-film (this work),

Cell components/properties	Parameters & symbols	Values
Cathode-4.4V NCM811	Specific capacity (C_0)	216 mAh g^{-1}
	Active material percentage (P_c)	97.5%
Al foil-12 μm	Areal density (ρ_{Al})	3.24×10^{-3} g cm^{-2}
	Factor (f_{Al}, including the Al pole)	1.06
Cu foil-4 μm	Areal density (ρ_{Cu})	3.60×10^{-3} g cm^{-2}
	Factor (f_{Cu}, including area redundancy and the Cu pole)	1.15
Separator-12 μm	Areal density (ρ_S)	0.646×10^{-3} g cm^{-2}
	Factor (f_S, Z-folded separator)	1.08
Al-plastic-film-88 μm	Areal density (ρ_P)	14.30×10^{-3} g cm^{-2}
	Factor (f_P, including the Ni, Al tabs and sealing edges)	4.09
Average voltage	U	3.84 V
Capacity utilization	R_i	100.0%
Relationship among C_c, R_e, n, and E	$C_c=\frac{-\left(\frac{32.011}{n}+4.4849\right)}{R_e-\frac{3840}{E}+4.748}$	
Relationship among C_c, R_e, and n (E = 500 Wh kg^{-1})	$C_c=\frac{-\left(\frac{32.011}{n}+4.4849\right)}{R_e-2.932}$	

When E=500 Wh kg^{-1}, n=10, R_e=1.5 g Ah^{-1}, we can obtain C_c=5.37 mAh cm^{-2}.

When E=508 Wh kg^{-1}, n=10, R_e=1.5 g Ah^{-1}, we can obtain C_c=5.61 mAh cm^{-2}.
This calculated result is consistent with home-made 2.7 Ah anode-free lithium pouch cells comprising a stack of 10 layers of cathodes and 11 layers of Cu foils.

Further increase the layer number to 20 (n=20, C_c=5.6 mAh cm^{-2}, R_e=1.5 g Ah^{-1}), the energy density of battery can be increased to be E=523.5 Wh kg^{-1}.

Supplementary Table 5 Physicochemical properties of LiDFOB/NDFA electrolytes at 25℃.

Concentration (mol L^{-1})	Molar ratio	Density (g cm^{-3})	Viscosity (mPa s)	Conductivity (mS cm^{-1})
0.5 M	1:15	1.2934	1.7328	7.41
0.8 M	1:12	1.3021	2.0513	7.82
1.0 M	1:9	1.3169	2.6876	7.34
1.6 M	1:5	1.355	7.0426	5.21
2.5 M	1:3	1.3964	26.968	2.35

Supplementary Table 6 Cell parameters of home-made 2.7 Ah anode-free lithium pouch cell.

Cell component	Parameter	Value
NCM811 Cathode	Specific capacity	216 mAh g^{-1}
	Active material percentage	97.5%
	Area weight (each side)	25.84 mg cm^{-2}
	Area capacity (each side)	5.6 mAh cm^{-2}
	Electrode length	5.6 cm
	Electrode width	4.3 cm
	Electrode areal	24.08 cm^2
	Thickness of Al foil	12 μm
	Weight of one layer	1359 mg
	Number of layers	10
	Weight	13.59 g
Cu foil	Thickness	4 μm
	Weight of one layer	99.7 mg
	Number of layers	11
	Weight	1.097 g
Separator	Thickness	12 μm
	Weight	0.37 g
Electrolyte	E/C ratio	1.5 g Ah^{-1}
	Weight	4.05 g
Package and Tabs	Weight	1.334 g
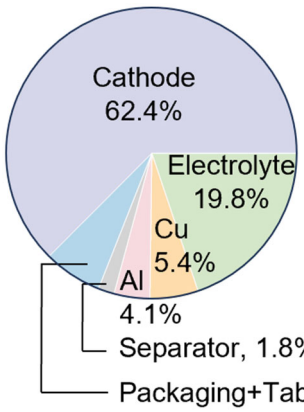	Average voltage	3.84 V
	Total capacity	2.7 Ah
	Total thickness	2.3 mm
	Energy	10.4 Wh
	Total weight	20.44 g
	Energy density	508 Wh kg^{-1}

Supplementary Table 7 Comparison of Ah-level high-energy-density anode-free Li pouch cells in literature and this work.

Electrolyte	Cell parameters					Energy density		Capacity retention	Reference
	Anode current collect	Cathode (mAh cm^{-2})	E/C (g Ah^{-1})	Capacity (Ah)	Stack layer	Stack-level (Wh kg^{-1})	Cell-level (Wh kg^{-1})		
2.0 M LiDFOB + 1.4 M $LiBF_4$ in FEC/DEC	Bare Cu	NCM523 2.75	2.6	0.21	7	365	N. A.	80% after 200 cycles	Nat. Energy 2020, 5, 693-702.
1.5 M LiFSI in DME/TTE	Bare Cu	NCM622 4.0	2.6	2.0	16	N. A.	350	80% after 100 cycles	Nat. Energy 2021, 6, 723-732.
1.0 M LiTFSI + 1.5 M LiFSI in G3/HFE	Bare Cu	NCM811 @L_2O 4.85	2.5	2.46	7	347	320	80% after 300 cycles	Nat. Energy 2021, 6, 653-662.
1.2 M LiFSI in F5DEE	Bare Cu	NCM523 3.1	2.4	0.2	7	N. A.	320	80% after 80 cycles	Nat. Energy 2022, 7, 94-106.
1.0 M $LiBF_4$ + 1.0 M LiDFOB tFEP/FEC	Bare Cu	NCM811 4.64	2.75	0.22	2	366	N. A.	80% after 100 cycles	Nat. Commun. 2023, 14, 1082.
1.4 M LiFSI in DME-HFC	Bare Cu	NCM523 2.92	2.5	0.2	7	342	323	80% after 82 cycles	Chem 2023, 9, 650-664.
1.0 M $LiPF_6$ in AN2-DME/FEC/TTE	Bare Cu	NCM811 4.25	3.0	0.125	2	398	N. A.	76% after 100 cycles	P. Natl. Acad. Sci. USA 2024, 121, e2316212121.
6.0 M LiFSI in DME	Bare Cu	Li_2NCM811 4.25	2.0	0.3	1	447	N. A.	93% after 50 cycles	Angew. Chem. Int. Ed. 2021, 60, 8289-8296
6.0 M LiFSI in DME	GaInSn Coating Cu	NCM811 4.25	2.0	0.125	1	420	N. A.	84% after 50 cycles	Adv. Energy Mater. 2021, 2003709
1.5 M LiFSI in DME/TTE	Bare Cu	NCM811 5.0	2.0	0.46	2	437	N. A.	70% after 74 cycles	Nano Lett. 2023, 23, 10251-10258.
1.6 M LiDFOB in NDFA (BAFF)	**Bare Cu**	**NCM811 5.6**	**1.5**	**2.7**	**10**	**543**	**508**	**80% after 100 cycles**	**This work**
	Bare Cu	**NCM811 5.6**	**1.5**	**2.15**	**10**	**434**	**406**	**80% after 250 cycles**	

Supplementary Table 8 Energy density and power density of home-made anode-free Li pouch cells and representative commercial energy storage devices.

Battery information	Energy density (Wh kg^{-1})	Power density (W kg^{-1})
Our AFLMB (2.7 Ah)	508	51
	478	96
	470	143
	459	229
	440	440
	412	825
	357	1262
	252	1679
	180	1998
	127	2356
	96	2650
LIB* (Panasonic power type, NCR18650PF–2.7 Ah), ref. [11]	206	44
	200	109
	194	214
	187	412
	177	780
	152	1104
	123	1371
	94	1475
	69	1566
LIB (Panasonic energy type, NCR18650BF–3.4 Ah), ref. [12]	248	27
	243	61
	230	115
	225	225
	190	400
	147	590
LTO batteries (LISHEN, LR60144TP–16 Ah), ref. [13]	55	55
	51	255
	49	489
	42	1147
	15	2557
Li-ion capacitors (JM Energy, 2000F–1.0 Ah), ref. [14]	11	110
	10	550
	9.5	810
	9	1200
	8.5	1400
	8.1	1600
	7.7	2300
Na-ion batteries (Li-FUN, 26700–S01–3.3 Ah), ref. [15]	113	23
	110	55
	107	107
Supercapacitors (Maxwell, BCAP3000, BCPA1500, BCAP1200, BCAP0650–0.25 Ah), ref. [16]	6	5900
	4.1	6800
	4.7	5800
	5.4	6600
Ni-MH batteries (Panasonic, BK260SCP–2.7 Ah), ref. [17]	58.9	218
	54	405
	49	588
	20	1500
	32.16	3.22

(Panasonic, LC-P127R2P–7.2 Ah), ref. [18]	30.2	6.04
	24.04	24.04
	21.2	42.4
	17	68
	11.4	136
	8.66	173.2

*The power density of Panasonic 18650 LIBs (power-type NCR18650PF-2.7 Ah) were tested in our laboratory. Our results are consistent with the open data from Panasonic company (see ref. [11]).

Supplementary references

1. Yu, Z. *et al.* Rational solvent molecule tuning for high-performance lithium metal battery electrolytes. *Nat. Energy* **7**, 94-106, (2022).
2. Qiao, Y. *et al.* A high-energy-density and long-life initial-anode-free lithium battery enabled by a Li_2O sacrificial agent. *Nat. Energy* **6**, 653-662, (2021).
3. Wu, Z. *et al.* Deciphering and modulating energetics of solvation structure enables aggressive high-voltage chemistry of Li metal batteries. *Chem* **9**, 650-664, (2023).
4. Louli, A. J. *et al.* Diagnosing and correcting anode-free cell failure via electrolyte and morphological analysis. *Nat. Energy* **5**, 693-702, (2020).
5. Mao, M. L. *et al.* Anion-enrichment interface enables high-voltage anode-free lithium metal batteries. *Nat. Commun.* **14**, 1082, (2023).
6. Niu, C. J. *et al.* Balancing interfacial reactions to achieve long cycle life in high-energy lithium metal batteries. *Nat. Energy* **6**, 723-732, (2021).
7. Lin, L. D. *et al.* Epitaxial Induced Plating Current-Collector Lasting Lifespan of Anode-Free Lithium Metal Battery. *Adv. Energy Mater.* **11**, 2003709, (2021).
8. Liu, L. & Wang, J. H. Overcoming Copper Substrate Thermodynamic Limitations in Anode-Free Lithium Pouch Cells via In Situ Seed Implantation. *Nano Letters* **23**, 10251-10258, (2023).
9. Günter, F. J. & Wassiliadis, N. State of the art of lithium-ion pouch cells in automotive applications: cell teardown and characterization. *J. Electrochem. Soc.* **169**, 030515, (2022).
10. Harlow, J. E. *et al.* A wide range of testing results on an excellent lithium-ion cell chemistry to be used as benchmarks for new battery technologies. *J. Electrochem. Soc.* **166**, A3031-A3044, (2019).
11. Datasheet. Technical Information of NCR18650PF LIB (2.7 Ah).
https://api.pim.na.industrial.panasonic.com/file_stream/main/fileversion/3447
12. Datasheet. Technical Information of NCR18650BF LIB (3.4 Ah).
https://www.master-instruments.com.au/file/63461/1/Panasonic-NCR18650BF.pdf
13. Datasheet. Technical Information of LISHEN LR60144TP Lithium-titanate batteries (16 Ah).
https://diysolarforum.com/resources/lishen-cell-datasheets.343/
14. Datasheet. Technical Information of JM Energy LIC Cell Performance (2000F, 1.0 Ah).
https://nccavs-usergroups.avs.org/wp-content/uploads/TFUG2009/2009_2banas.pdf
15. Datasheet. Technical Information of Li-FUN Na-ion batteries (3.3 Ah).
https://new.qq.com/rain/a/20231218A05YAR00
16. Datasheet. Technical Information of Maxwell Supercapacitors (0.25 Ah).
https://www.keenlab.de/wp-content/uploads/2020/02/K2Series_DS_1015370_5_20141104.pdf
17. Datasheet. Technical Information of Panasonic BK260SCP Ni-MH batteries (2.7 Ah). (0.25 Ah).
https://industrial.panasonic.com/cdbs/www-data/pdf2/ACG4000/ACG4000CE272.pdf
18. Datasheet. Technical Information of Panasonic LC-P127R2P Lead-acid batteries (7.2 Ah).
https://files.dcpower.eu/datasheets/panasonic/LC-R127R2PG.pdf